Sea-level oscillations within the Last Interglacial: insights from coral reef stratigraphic forward modelling

Denovan Chauveau[a*], Nikos Georgiou[a], Ciro Cerrone[a], Silas Dean[a], Alessio Rovere[a,b]

[a]*Department of Environmental Sciences, Informatics and Statistics, Ca' Foscari University of Venice, Italy*

[b]*MARUM, Center for Marine Environmental Sciences, University of Bremen, Germany*

**Corresponding author:* denovan.chauveau@unive.it

Sea-level oscillations within the Last Interglacial: insights from coral reef stratigraphic forward modelling

Denovan Chauveau[a], Nikos Georgiou[a], Ciro Cerrone[a], Silas Dean[a], Alessio Rovere[a,b]

[a]*Department of Environmental Sciences, Informatics and Statistics, Ca' Foscari University of Venice, Italy*

[b]*MARUM, Center for Marine Environmental Sciences, University of Bremen, Germany*

Keywords

Marine Isotope Stage 5e; Last Interglacial; Sea level; Fossil coral reef; Stratigraphic forward modelling

Abbreviations

Marine Isotope Stage (MIS); Greenland Ice Sheet (GrIS); Antarctic Ice Sheet (AIS); Global Mean Sea Level (GMSL); Relative Sea Level (RSL); Coral Reef Terrace (CRT)

Abstract

Understanding past sea-level variations is essential to constrain future patterns of sea-level rise in response to warmer climate conditions. Due to good preservation and the possibility to use various geochemical methods to date fossil sea-level index points, the Last Interglacial (Marine Isotope Stage, MIS, 5e, 130-116 ka) is often regarded as one of the best climate analogs for a future warmer climate. MIS 5e coastal stratigraphic sequences, such as fossil coral reefs in tectonically stable areas, are characterized by abrupt shifts in their geological facies, steps within the reef topography or backstepped fossil reefs, which have been often interpreted as proxies for abrupt sea-level fluctuations within the interglacial. However, the observational evidence and magnitude of such abrupt changes are controversial. Here, we run nearly 50 thousand simulations of a 2D kinematic reef model that can reproduce coral reef growth and demise through time. Our aim is to investigate the parameters of space, the sea-level scenarios, and the processes which multiple-stepped MIS 5e fossil reefs form. As inputs to the model, we use both published and synthetic sea-level histories (17 sea-level curves ranging from one to several sea-level peaks), and a wide range of reef growth rates, marine erosion rates and bedrock foundation slopes. Our results show that the only sea-level history that could explain the generation of an emerged MIS 5e backstepped reef is a first sea-level peak followed by an abrupt rise in sea level and a second short-term peak. Any other multiple-stepped stratigraphy can be explained by the interplay between reef growth, marine erosion, and bedrock slope.

1. Introduction

In less than a century, global atmospheric temperatures will likely be 2°C higher than in the pre-industrial period (Raftery et al., 2017), leading to a sea-level rise up to 1 m by 2100 (high-end SSP5-8.5 scenario from the AR6 Intergovernmental Panel on Climate Change, IPCC; Fox-Kemper et al., 2021). In this context, it is crucial to constrain future fluctuations in sea level to rapidly draw up adaptation plans. Substantial uncertainties regarding future sea-level scenarios are related to the response of the Greenland and Antarctic Ice Sheets (GrIS and AIS) to global warming (Horton et al., 2020). DeConto et al. (2021) show that melting pulses caused by AIS retreat could lead to sea-level rise rates an order of magnitude higher than today. To accurately assess the current instability of ice sheets, it is crucial to enhance our understanding of past meltwater pulses during fast sea-level transgressions (Liu et al., 2015) and interglacials (Deiana et al., 2021).

The Last Interglacial (Marine Isotope Stage, MIS, 5e, 130-116 ka ago) was the last period of the Earth's history when the climate was warmer than pre-industrial. As a result, MIS 5e ice sheets were smaller than today, and global mean sea level (GMSL) was 2-9 m above present mean sea level (e.g., Dutton & Lambeck, 2012; Dyer et al., 2021; Dumitru et al., 2023). The existence and possible patterns of abrupt GMSL changes within MIS 5e

are still debated (Dutton & Barlow, 2019). Indeed, several coastal features associated with MIS 5e are characterized by abrupt shifts in geological facies (see Section 2), that many authors attributed to rapid relative sea-level (RSL) changes or fluctuations within the interglacial (Hearty et al., 2007; O'Leary et al., 2013; Vyverberg et al., 2018). One critical point is that these proxies, mainly from coral reef areas, are subject to several uncertainties, stemming from the dating and interpretation of paleowater depth of fossil corals (Hibbert et al., 2016; Polyak et al., 2018). This limits our ability to draw conclusions about possible MIS 5e GMSL fluctuations (Dutton & Barlow, 2019).

Multi-meter GMSL fluctuations (e.g., low-to-high swings of more than 4 m, Thompson et al., 2005; Kopp et al., 2009) would entail ice regrowth during the Last Interglacial, which is considered highly unlikely as there are no plausible processes that could explain it (Barlow et al., 2018). Non-eustatic processes have been invoked to explain MIS 5e coastal stratigraphies showing signs of possible intra-interglacial sea-level fluctuations, including local tectonic movements (Whitney & Hengesh, 2015) or the effect of topographical variations of antecedent foundations on new reef constructions (Chauveau et al., 2023). Another plausible explanation is that AIS and GrIS evolved asynchronously during MIS 5e and then contributed to GMSL at different times. This would result in an early sea-level highstand (before 125 ka) stemming from AIS melting, followed by a later and more diffuse contribution from GrIS (Rohling et al., 2019; Barnett et al., 2023).

In this study, we use a numerical model (REEF, Husson et al., 2018; Pastier et al., 2019) that simulates the growth and erosion of coral reefs through time to investigate the effects of different sea-level histories on their formation during the Last Interglacial. As inputs to the model, we use both published and synthetic sea-level histories, and a wide range of input parameters (i.e., reef growth rate, marine erosion rate and bedrock foundation slope). We ran a total of nearly 50 thousand numerical simulations. We discuss which MIS 5e GMSL conditions are most favorable for the development of stratigraphic and morphological characteristics that may be interpreted as evidence for sea-level fluctuations during the interglacial.

2. Background: Fossil coral reefs

Living and fossil corals are widespread around the world's tropical and subtropical areas (Veron et al., 2015; Chutcharavan & Dutton, 2021). Coral reef genesis is strongly influenced by the accommodation space, which corresponds to the interplay between sea-level changes and reef growth, as well as the slope of bedrocks and their availability for coral settlement (Camoin & Webster, 2015). When the sea level falls too rapidly, coral reefs may emerge and die, creating coral reef terraces (CRTs, Murray-Wallace & Woodroffe, 2014). CRTs are expanses of reefal limestone (i.e., the fossil coral-built surfaces) with flat or slightly sloping surfaces, limited seaward

by a distal edge over a cliff of variable thickness (e.g., Chappell, 1974; Fig. 1A). Landward, CRTs are limited by an inner edge, characterized by a break in slope (Fig. 1).

The morphology and stratigraphy of CRTs are the result of the interactions between reef accretion (bioconstruction and sedimentation), RSL changes, erosion (marine and continental) and the basement geometry (Camoin & Webster, 2015; Pastier et al., 2019; Chauveau et al., 2021), resulting in a wide spectrum of morphologies (Pedoja et al., 2018). Complex stratigraphic contexts associated with reefs formed during a single highstand have been described both in tectonically stable (e.g., Chen et al., 1991) and uplifting areas (Pedoja et al., 2014). For example, there may be several morphologically distinct CRTs (Fig. 1B, 1C; e.g., de Gelder et al., 2022); reefal limestone units of slightly different ages within a single CRT (Fig. 1B; Chauveau et al., 2021) or separated by an erosional surface or layer of coral rubble (e.g., Thompson et al., 2011); changes in reef facies (e.g., Bruggemann et al., 2004); or the backstepping of the reef crest (Fig. 1C; e.g., Blanchon, 2010). All these features have been described at several locations globally (see the compilation in Hearty et al., 2007, Rohling et al., 2019, and Dutton et al., 2022), but their origin is still controversial.

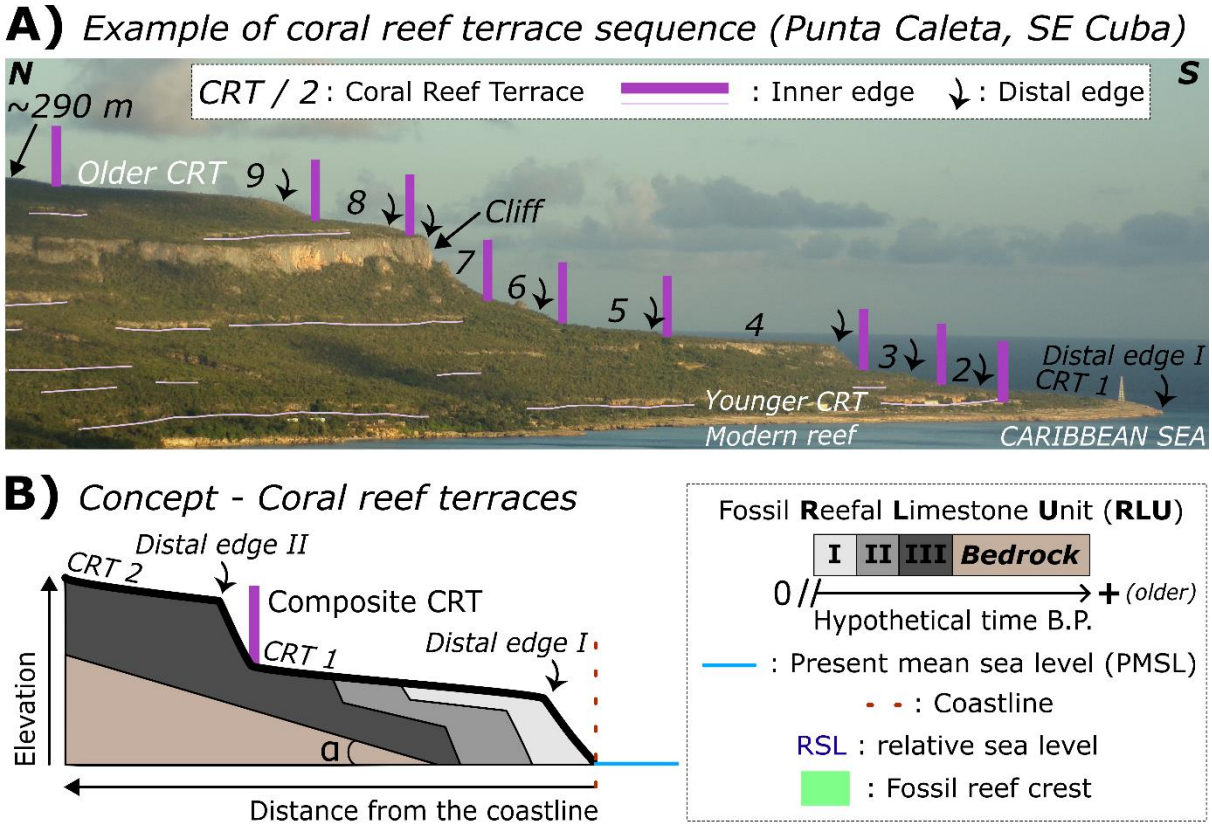

Figure 1. A) *View from the west of Punta Caleta (south-east Cuba). The coral reef terrace sequence visible in the image is around 1.5 kilometers long. The inner edges drawn on the image are only those visible and therefore do not represent all of those mapped by Peñalver et al. (2021). The highest terrace in this area is estimated to be several million years old (Authemayou et al., 2023). The cliff shown in the image is the highest in the sequence. Schematic concept of* **B)** *a CRT including several reefal limestone units and* **C)** *a backstepped fossil coral reef. The process of backstepping consists of the abrupt demise of a reef (CRT 1) and the*

construction of a new reef surface (CRT 2), topographically higher than the previous one (Blanchon, 2010; Camoin & Webster, 2015). The cause of reef backstepping is a rapid rise in RSL (elevation d', i.e., the difference between RSL1 and RSL2), which drowns the older reef and prevents coral growth due to the RSL rising faster than the reef growth rate. CRTs 1 and 2 may be separated by relatively long distance (d; e.g., Blanchon, 2010).

3. Methodology: Fossil coral reef modeling

Coastal landscape evolution models can be used to assess the geometry of a marine terrace sequence, to constrain the chrono-stratigraphy, and to unravel the influence of processes involved in their morphogenesis (de Gelder et al., 2020; Georgiou et al., 2022; Matsumoto et al., 2022; Boyden et al., 2023). Since the pioneering work of Chappell (1980), several numerical models of reef growth have been developed (Turcotte & Bernthal, 1984; Bosscher & Schlager, 1992; Webster et al., 2007; Koelling et al., 2009; Toomey et al., 2013). Here, we use the kinematic Fortran code model REEF, developed by Husson et al. (2018) and Pastier et al. (2019). REEF is a profile evolution model that considers past eustatic sea-level oscillations, vertical land motion, reef growth, marine erosion, and the resulting deposition of the eroded clastic sediments, modelling on an initially linear slope.

Reef growth in REEF is defined through a potential reef growth rate, consisting of a vertical component of aggradation (accounting for the decreasing coral growth rate with increasing depth as a response to light attenuation) and a horizontal component of progradation (considering the decreasing coral growth from the reef crest, facing the open sea, towards the shore). Marine erosion is based on the wave erosion model of Anderson et al. (1999). It integrates a vertical seabed erosion component as well as a horizontal cliff erosion component. In the REEF model, these are approximated by an eroded volume, in which the proportions between vertical and horizontal erosions rely on wave dissipation (Anderson et al., 1999). Clastic sediment deposition reflects the eroded rock volume, in which horizontal deposition occurs in reef flats or inner lagoons if any (i.e., several meters deep, e.g., Kennedy et al., 2021), and at a repose angle of 10% at the base of the forereef slope. The temporal and spatial resolution are respectively 1 ka and 1 m. We refer the reader to Husson et al. (2018), Pastier et al. (2019), and Chauveau et al. (2023) for more details about REEF code.

Our approach aims to constrain the parametric conditions with which the REEF model can recreate multiple CRTs associated with MIS 5e, and ideally to recreate a younger unit on top of an older one, in a hypothetical case of a tectonically stable area. For this purpose, we free the model from tectonics as input and use a wide range of values for each parameter (Table 1). These ranges have been chosen on the basis of previous studies (maximum reef

197 growth rate, Dullo, 2005; bedrock slope, Chen et al., 1991, Rovere et al.,
198 2018), to study extreme cases (maximum reef growth rate of 50 mm a^{-1})
199 or because very few constraints exist (erosion rate; see Section 5.2.). To
200 simulate reef growth and demise under different sea-level scenarios we use
201 different GMSL curves from the following sources: Waelbroeck et al. (2002),
202 Bintanja et al. (2005), Kopp et al. (2009), Rohling et al. (2009), Spratt &
203 Lisiecki (2016), Rohling et al. (2019), and Dumitru et al. (2023) (Fig. 2A,
204 see the description of these curves in the supplementary information,
205 Section SI.1.). In addition to these proxy-based GMSL curves, we also
206 created synthetic sea-level scenarios that reproduce intra-interglacial
207 fluctuations (Fig. 2B, 2C, 2D). These synthetic curves have a duration of 15
208 ka. The maximum and the minimum ages are set because they correspond
209 to the most widely accepted age limits: 130 ka (Rohling et al., 2019) and
210 116 ka (Rovere et al., 2016; Dutton & Barlow, 2019), respectively. This
211 time step also makes it possible to create sea-level curves with an axis of
212 symmetry at 123 ka (Fig. 2B, 2C, 2D). These synthetic curves have a
213 maximum amplitude variability of 18 m (i.e., between -9 and 9 m relative
214 to present sea level) to consider the maximum sea-level value at MIS 5e
215 (e.g., Kopp et al., 2009, 2013; Dutton & Lambeck, 2012). In total, we ran
216 49980 simulations (2940 per each single sea-level scenario) using
217 permutations of the parameters shown in Table 1. To gauge the ability of
218 each simulation to reproduce a scenario of multiple fossil CRTs, we adopt a
219 score based on 3 criteria, as shown in Table 2.

Symbol	Definition	Permuted value(s)	Unit
α	Initial bedrock slope	1, 2, 3, 4, 5, 6, 8, 10, 15, 20, 25, 30, 40, 50	%
G_{max}	Maximum reef growth rate	1, 2, 3, 4, 5, 6, 8, 10, 15, 20, 25, 30, 40, 50	mm a^{-1}
E	Erosion rate	1, 5, 10, 20, 30, 40, 50, 60, 80, 100, 150, 200, 300, 400, 500	mm^3 a^{-1}
Z_{max}	Maximum reef growth depth	20	m
Z_{min}	Optimal reef growth depth	2	m
Z_0	Maximum depth of wave erosion	3	m

Table 1. *Model input parameters, symbols, values, and units. The minimum possible value as model input for all parameters is 1. The maximum and optimal reef growth depths (Z_{max} and Z_{min}, respectively) and the maximum depth of wave erosion (Z_o) are based on previous studies: 20 m, 2 m (Bosscher & Schlager, 1992) and 3 m (Pastier et al., 2019), respectively.*

Criterion	Definition	Total point
0	Submerged CRT	0
I	One emerged CRT or reefal limestone unit	1
II	Multiple emerged CRTs	2
III	The youngest CRT is above the oldest CRT	3

Table 2. *Criteria for scoring simulations. When the reef reproduced by a simulation fills a criterion, the simulation is scored with 1 point. The maximum score attainable is 3 points.*

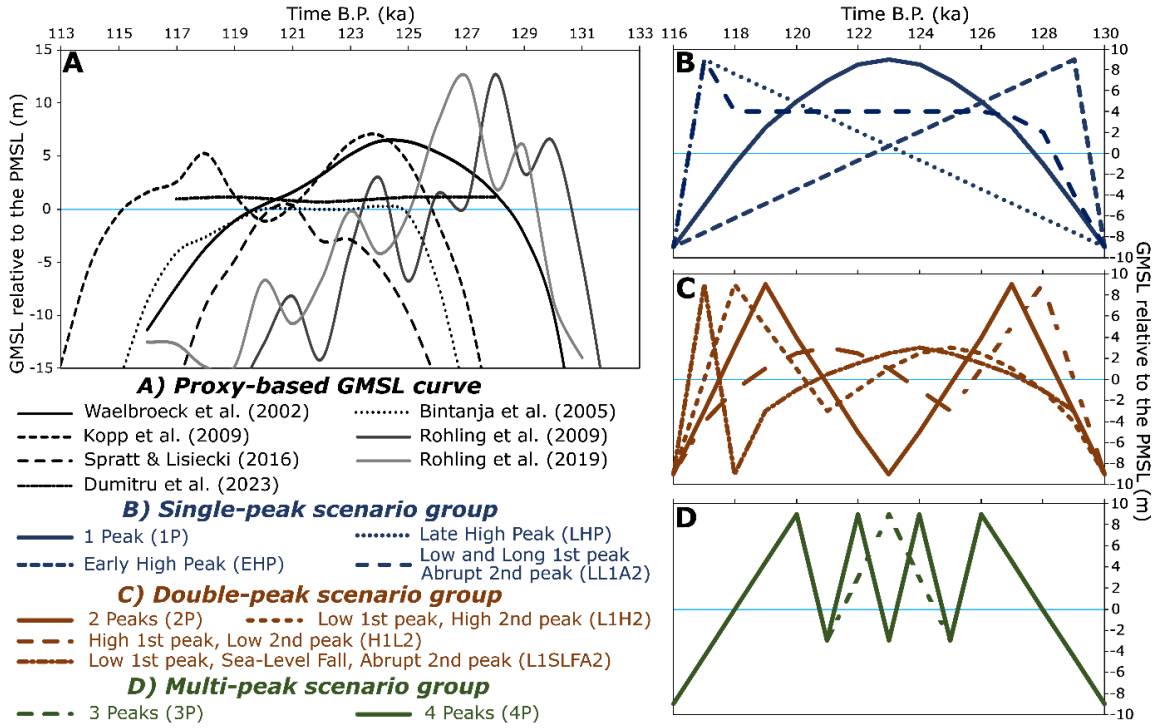

Figure 2. *Sea-level scenarios for the MIS 5e used in this study as inputs in the model of Pastier et al. (2019):* ***A)*** *proxy-based GMSL curves, and synthetic sea-level curves divided in three groups:* ***B)*** *Single-peak,* ***C)*** *Double-peak,* ***D)*** *Multi-peak GMSL scenarios. The sea-level curves are relative to the present mean sea level (PMSL). The sea-level curves of Kopp et al. (2009) and Dumitru et al. (2023) are the 50th percentile predictions provided by these authors. The sea-level curve of Rohling et al. (2019) is the same as that shown in Figure 3a of this article (i.e., GMSL approximation based on the probabilistically assessed KL11 Probability maximum, PM; see Section SI.1). The single-peak group includes 1) one major peak (1P); 2) a relatively stable sea level with a late peak (LHP), or 3) an early peak (EHP); 4) a first flat, relatively long and low peak, followed by a second relatively high and short peak, separated by an abrupt rise in sea level (LL1A2); The double-peak group includes 5) two peaks separated by high sea-level fall (2P); 6) a first relatively low and long peak followed by a sea-level drop and*

a second higher and shorter peak (L1H2); 7) a first relatively high and short peak followed by a lower and longer peak (H1L2); 8) a first relatively low and long peak followed by a second shorter and higher peak, both separated by an abrupt sea-level drop (L1SLFA2); and the multi-peak group includes 9) 3 and 10) 4 peaks. In this study, we consider the length of a sea-level peak to be the time between the start of the transgression and the end of the regression surrounding the sea-level maximum.

As the model does not simulate reef facies, we consider a reefal limestone unit to be a unit constructed over 1 ka (i.e., the model time step). A CRT/reefal limestone unit is considered emerged when it is higher than 1 m above present sea level (i.e., corresponding to the uncertainty of the model, Fig. 3A). We consider that the model output has two CRTs when they are separated by a significant slope (i.e., greater than 5%), associated with a cliff of more than 1-m high, overhanging the inner edge (Fig. 3B, 3C). Given the very wide parametric range and the time step of 1 ka, sometimes, the simulations produce morphologies that are not realistic, i.e., morphological surface with concavities of over 1 m. This is primarily because of the 1 ka time step, coupled with excessively high reef growth and insufficient erosion rates. When such emerged irregularities are more than 1 m thick, we consider only criterion I to be valid in order to select only the most realistic simulations.

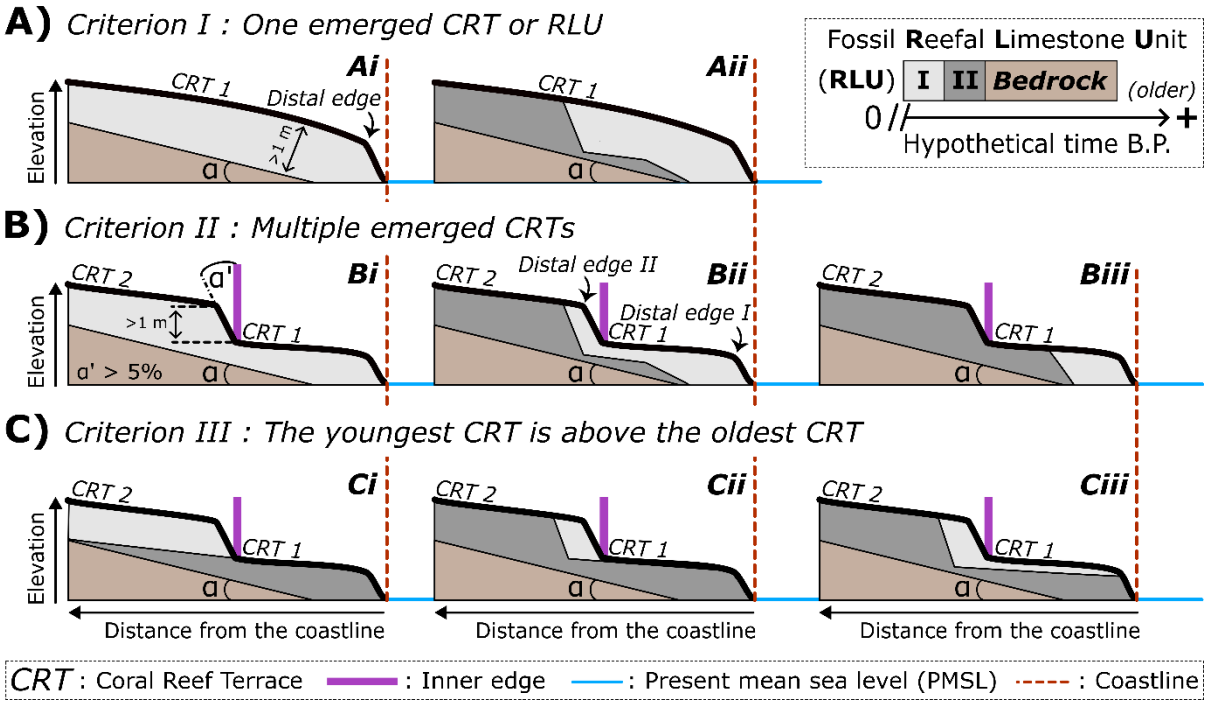

***Figure 3**. Schematic example of different chrono-morphology scenarios that validate criteria **A)** I: One emerged CRT or reefal limestone unit, **B)** II: Multiple emerged CRTs, **C)** III: The youngest CRT is above the oldest CRT. Elevations and distances not to scale. Criterion III is valid even if the terraces contain several reefal limestone units, as in Cii-iii.*

4. Results

Of the 49980 simulations, 2 proxy-based GMSL curves (i.e., from Bintanja et al., 2005 and Spratt & Lisiecki, 2016), representing 12% of our simulations (5880 simulations), were discarded from further analysis, as they scored zero (Fig. 4). Out of the remaining 44100 simulations, 7% reached a score of zero (3252 simulations), 75% a score of 1 (33242 simulations), 16% a score of 2 (6875 simulations) and 2% (731

simulations) reached a score of 3 (Fig. 4). In the supplementary information (Section SI.2.), we describe all the results as well as parametric trends for the proxy-based GMSL (Fig. SI1) and synthetic sea-level curves (Figs. SI2; SI3; SI4) scenarios. Below, we describe the set of morphologies obtained by simulations reaching scores of 3 and 2, and then discuss the relationship between marine erosion rate and initial bedrock slope.

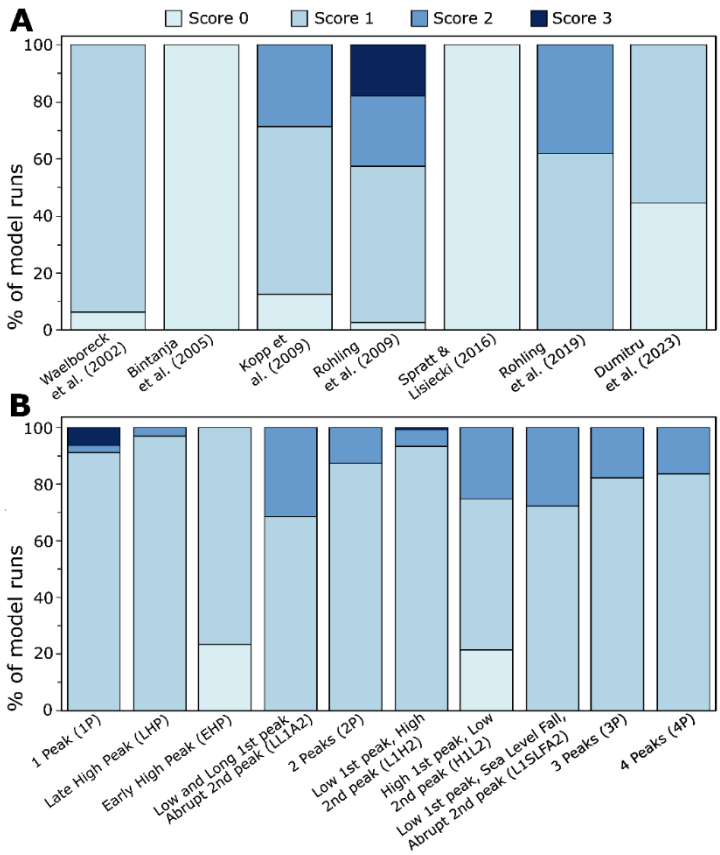

Figure 4. *Percentage of scores for the* ***A)*** *proxy-based and* ***B)*** *synthetic sea-level curves.*

4.1. The youngest CRT is above the oldest CRT (Score of 3)

On the 44100 simulations, 731 reached a score of 3. Among these, 72% have as input the multi-peak GMSL curve of Rohling et al. (2009) (523

simulations). The other high scores are attained by synthetic sea-level curves, 25% of those with one major peak (i.e., 1P, 183 simulations) and 3% among the Low 1st peak, High 2nd peak (i.e., L1H2, 25 simulations) scenarios.

Some simulations from the GMSL curve of Rohling et al. (2009) show the abrupt demise of CRTs (Fig. 5A, 5B). In these cases (Fig. SI1), a reef is first demised (at 131 ka) and another reef is built higher up (from 131 to 130 ka ago, Fig. 5B). This new reef is then demised (at 129 ka), to make way for a new 129/128 ka reef built during the sea-level maximum of this scenario (2nd peak), around 7 m higher up and at around 400 m landward (Fig. 5B). During this period, a reef veneer reoccupies the 131/130 ka fossil reef (Fig. 5B). This thin coral layer is then eroded during the subsequent sea-level oscillations (Fig. 5C, 5D). Finally, the two CRTs (1 and 2, Fig. 5E, 5F) emerge during the following sea-level regression. The simulations, that successfully reproduce the backstepping process (Fig. SI1), are all in the range of α (initial bedrock slope) = [1-15] % and E (erosion rate) = [20-500] mm^3 a^{-1} and are only valid for G_{max} (maximum reef growth rate) = 1 mm a^{-1} (Fig. SI1).

313

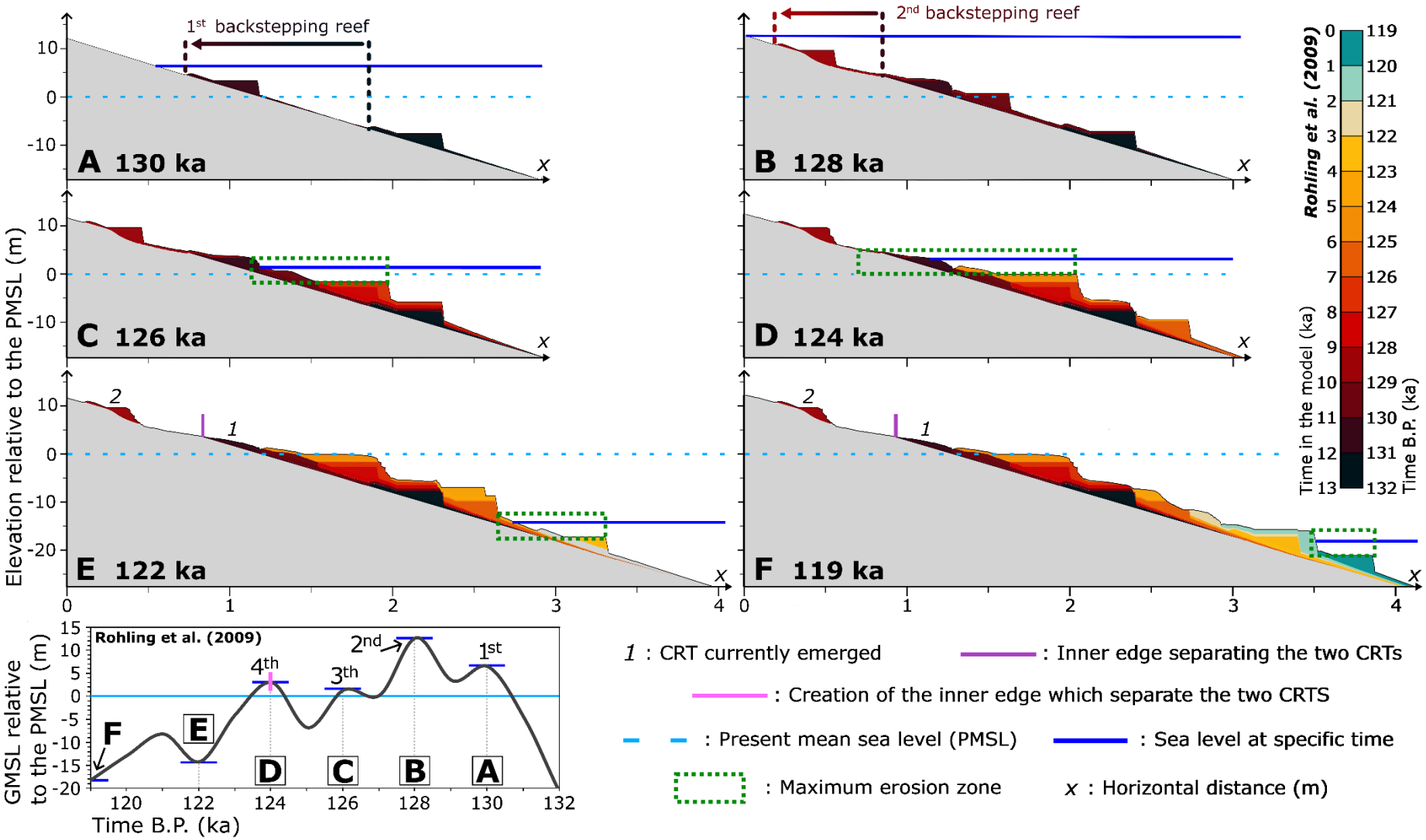
1st backstepping reef
2nd backstepping reef
A 130 ka
B 128 ka
C 126 ka
D 124 ka
E 122 ka
F 119 ka
Elevation relative to the PMSL (m)
Rohling et al. (2009)
Time in the model (ka)
Time B.P. (ka)
GMSL relative to the PMSL (m)
Rohling et al. (2009)
1st
2nd
3th
4th
Time B.P. (ka)
1 : CRT currently emerged
: Inner edge separating the two CRTs
: Creation of the inner edge which separate the two CRTS
: Present mean sea level (PMSL)
: Sea level at specific time
: Maximum erosion zone
x : Horizontal distance (m)

Figure 5. *Formation of coral reef terraces with the GMSL curve of Rohling et al. (2009) at different steps:* ***A)*** *130,* ***B)*** *128,* ***C)*** *126,* ***D)*** *124,* ***E)*** *122,* ***F)*** *119 ka ago. These steps are placed by the dark blue line on the sea-level curve at the bottom left. The parameters of the selected simulation are as follows: α (initial bedrock slope) = 1%, G_{max} (maximum reef growth rate) = 1 mm a^{-1}, E (erosion rate) = 400 mm^3 a^{-1}. The maximum erosion zone is 5 m relative to the sea level at the specific time (3 m below and 2 m above). The 5 m value corresponds to the maximum depth of wave erosion (i.e., 3 m; Table 1), plus cliff erosion (i.e., 1 m, Pastier et al., 2019), plus model uncertainty (i.e., 1 m). As the model does not simulate reef facies such as the reef crest, we take the inner edges as the reference for the backstepping process.*

The simulations with score 3 from the one major peak scenario (1P) all show the same morphological characteristics: a large, high emerged CRT (around 7 m above the present mean sea level) with age of 126/125 ka (Fig. 6B). Below this, a second, less wide CRT of an older age is formed (i.e., 127/126 ka; Fig. 6B) emerging around 3 m above the present mean sea level. This type of double CRT is also found with the GMSL curve of Rohling et al. (2009) for G_{max} values > 5/6 mm a^{-1}.

The simulations that reach the score of 3 with the L1H2 scenario (i.e., a first relatively low and long peak followed by a sea-level drop and a second higher and shorter peak) all show two CRTs emerged around 3 m and 6 m

above the present mean sea level (Fig. 6C). The lowest contains two reefal limestone units of ages 120/119 ka and 119/118 ka. The highest CRT is made up of the youngest reefal limestone unit (i.e., age of 119/118 ka; Fig. 6C).

The inner edges are formed much later than the creation of the highest CRT: 4, 8 and 2 ka later for the GMSL curve of Rohling et al. (2019), the 1P and L1H2 scenarios, respectively (Figs. 5; 6). In the case of the GMSL curve of Rohling et al. (2009), it is the erosion during the fourth sea-level peak (124 ka ago, Fig. 5) that creates the inner edge that is now emerged (Figs. 5E, 5F), by eroding the coral veneer (built at 131/130 ka) as well as the lowest emerged CRT (Fig. 5D).

With the 1P and L1H2 sea-level scenarios, it is the sea-level regression following the maximum sea-level peak that will erode the previously emerged CRT, outcropping older reefal limestone units below more recent ones. For example, the long sea-level peak with a relatively stable sea level of the 1P (Figs. 3B; 6D) scenario allows the construction of a large reef that saturates the accommodation space from the first half of MIS 5e (up to 123 ka). Then, during the slow, unabrupt sea-level regression (from 123 ka; Figs. 3B; 6D), the first reefal limestone unit is eroded and an older one emerges. The same process applies to scenario L1H2 (Fig. 6C) but with a different timing (Fig. 6D). Thus, all the inner edges generated with the 3-score simulations are erosive ones. These are characterized by a time-lapse

that distinguishes them from the creation of the surrounding CRTs (Fig. 6D). Thus, while the sea-level rise rate seems to play an important role in the formation of backstepped reefs (Figs. 5, 6A), this does not seem to be the case for the formation of double CRTs, which is mainly explained by the action of erosion (Figs. 6B, 6C, 7).

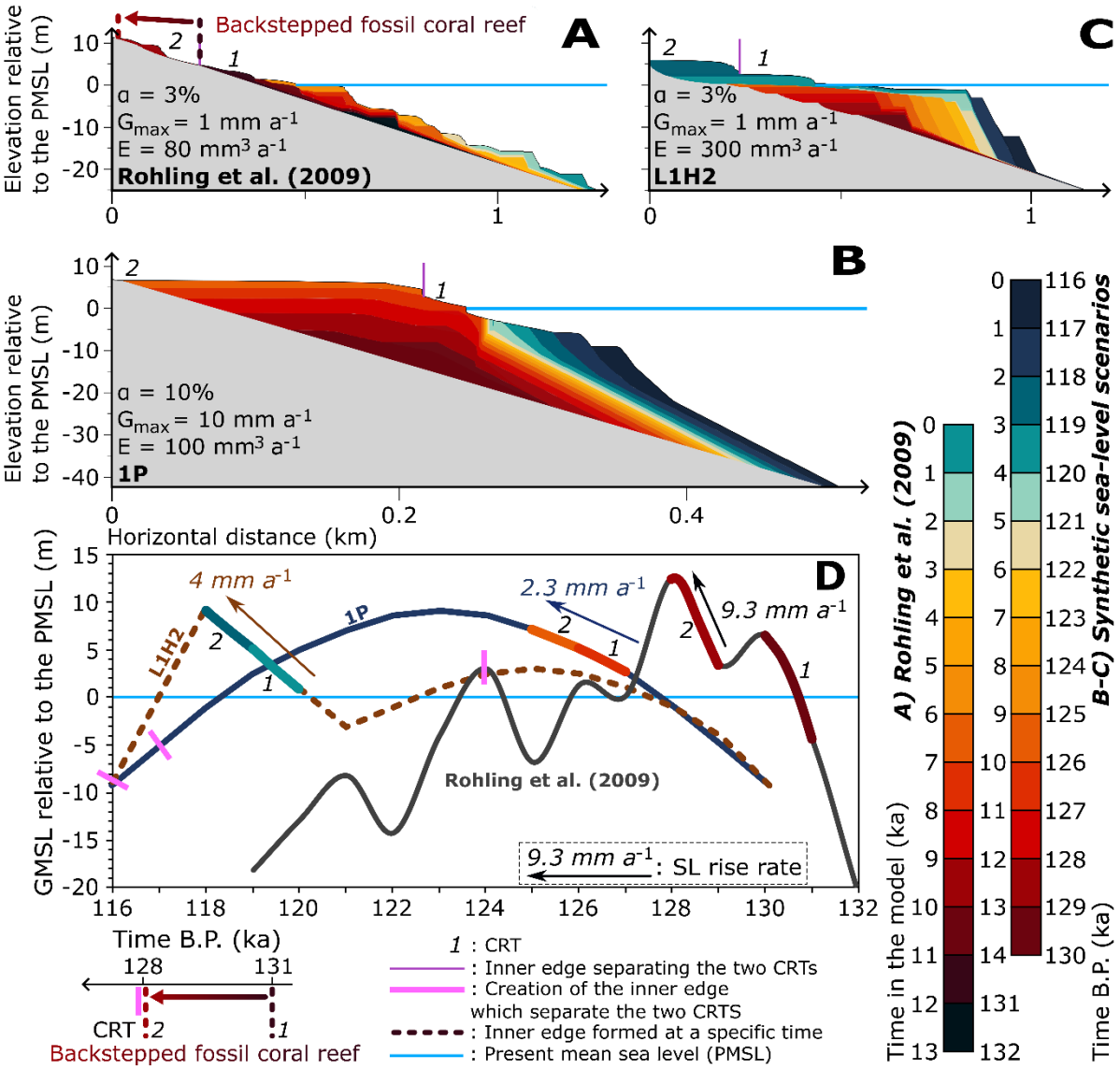

Figure 6. Example of simulations that reached the maximum score of 3. Simulations from the GMSL curve of **A)** Rohling et al. (2009), and the synthetic sea-level scenarios **B)** 1P and **C)** L1H2 (see Fig. 2). As the model does not simulate reef facies such as the reef crest, we take the inner edges as the reference for the backstepping process. **D)** Sea-level scenarios listed above. The pink lines mark the age at which the inner edge separating the two CRTs of different ages is created. Elevations are given relative to the present mean sea level (PMSL).

4.2. Multiple emerged CRTs (Score of 2)

Of the 15 sea-level scenarios (without considering the ones of Bintanja et al., 2005 and Spratt & Lisiecki, 2016), 12 have simulations with a score of 2, representing 16% of the total simulations. Thus, a wide range of scenarios can create a multiple coral reef record: single-peak scenarios (1P, LL1A2, LHP; Figs. 6; 7; SI2) as well as double/multi-peak scenarios (Kopp et al., 2009, Rohling et al., 2009, 2019, 2P, L1H2, H1L2, L1SLFA2, 3P, 4P; Figs. 6; 7; SI1; SI3; SI4).

This leads to a vast array of modelled reef morphologies (Fig. 7): an older CRT above a more recent one, both including a single reefal limestone unit (Kopp et al., 2009, LHP; Fig. 7A, 7C); a unique reefal limestone unit forming two CRTs (Rohling et al., 2019, LL1A2, 2P, L1SLFA2; Fig. 7B, 7D, 7F, 7G);

two CRTs, each composed of several reefal limestone units (H1L2, 4P, 3P; Fig. 7F, 7I, 7H); and three distinct CRTs (2P, 3P; Fig. 7E, 7H).

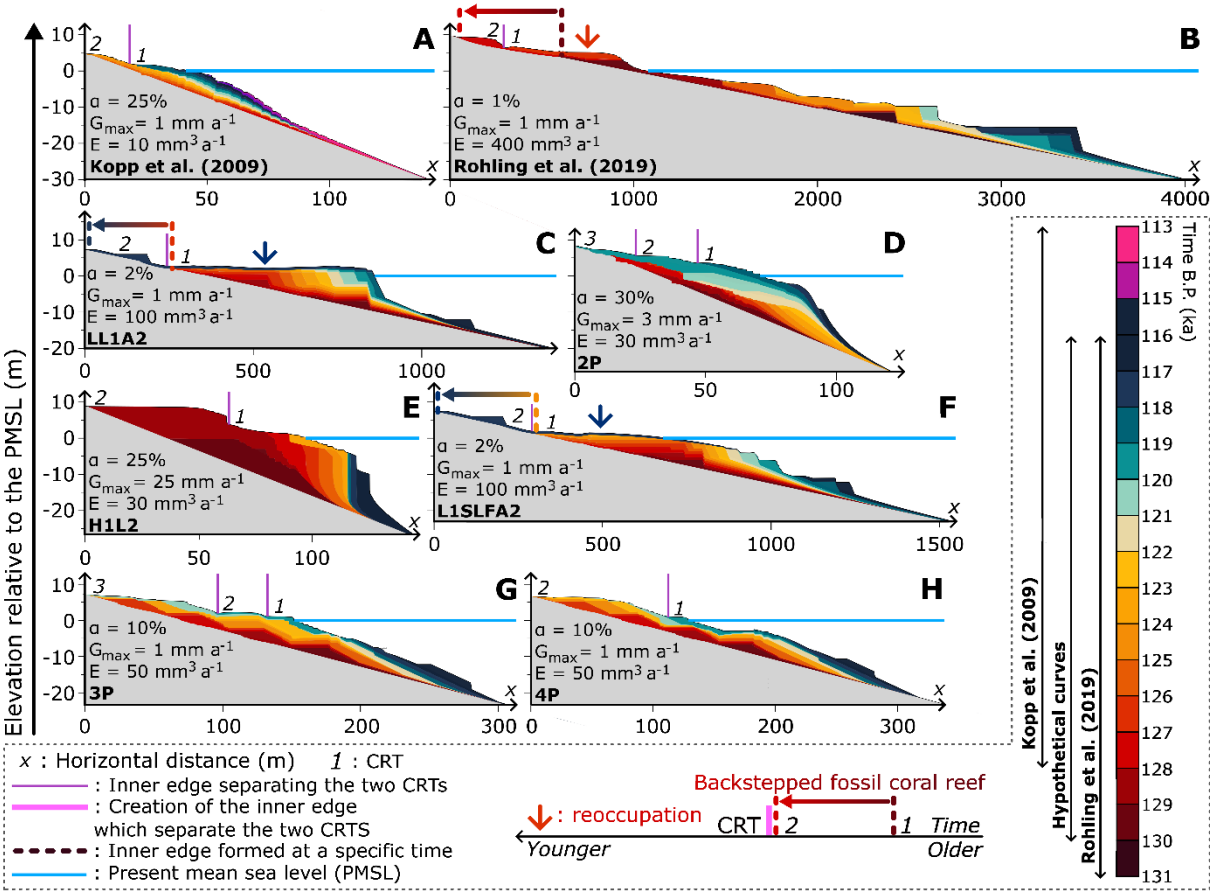

Figure 7. *Example of simulations that reached the score of 2, i.e., simulating multiple CRTs but with an older CRT on top. Simulations from the GMSL curve of* ***A)*** *Kopp et al. (2009),* ***B)*** *Rohling et al. (2019), and the synthetic sea-level scenarios* ***C)*** *LL1A2,* ***D)*** *2P,* ***E)*** *H1L2,* ***F)*** *L1SLFA2,* ***G)*** *3P, and* ***H)*** *4P (see Fig. 2). As the model does not simulate reef facies such as the reef crest, we take the inner edges as the reference for the backstepping process. The color of the arrows marking the reoccupation corresponds to the time at which the reoccupation took place. Elevations are given relative to the present mean sea level (PMSL).*

Three scenarios (Rohling et al., 2019; LL1A2 and L1SLFA2) have almost succeeded in reproducing the backstepping process (Fig. 7B, 7D, 7F). However, the last criterion was not validated because the lower CRT is systematically reoccupied by a coral layer of the same age as the upper CRT (Fig. 7A, 7D, 7G). In the case of the GMSL of Rohling et al. (2019), the sea-level peak creating the upper backstepped reef (from 128 to 124 ka; Fig. 2A) is 2 ka longer than that of the GMSL of Rohling et al. (2009) (from 129 to 127 ka; Fig. 2A). This longer time allows the youngest reef (128-127 ka; Fig. 7B) to reoccupy the oldest by a coral layer several meters thick (129-128 ka; Fig. 7B), as opposed to the veneer layer constructed with the GMSL curve of Rohling et al. (2009) (Fig. 5B).

The length of the highest 2nd peak is the same between the sea-level scenarios LL1A2, L1SLFA2, and the GMSL of Rohling et al. (2009), i.e., 2 ka, and its relative elevation with respect to the lowest 1st peak differs only slightly (from 5 to 6.3 m, Fig. 2A, 2B, 2C). However, the first two scenarios show a reef layer reoccupying the lowest CRT (Fig. 7C, 7F), whereas the last does not (Figs. 5E, 5F; 6A). This is because the LL1A2 and L1SLFA2 scenarios stop after the 2nd peak, whereas the GMSL curve of Rohling et al. (2009) continues and experiences two further sea-level peaks above the present mean sea level (at ~126 and ~124 ka, respectively, Figs. 2A; 5; 6D), leading to erosion of the previously formed reoccupation layer (Fig. 5D). As a result, with a longer and more complex eustatic history, the LL1A2 and L1SLFA2 scenarios would very likely have achieved a score of 3.

4.3. Relationship between bedrock slope and marine erosion

Our results highlight the maximum efficiency of marine erosion, which we consider here as the potential of nearshore processes to erode an emerged CRT. In general, marine erosion increases with the increase of the initial bedrock slope α (Figs. 8; SI1; SI2; SI3; SI4). In other words, the greater the bedrock slope, the more easily and quickly the emerged CRT will be eroded, whatever the sea-level scenario (Fig. 8).

We note a strong correlation (R_{mean}^2 = 0.99) with a second-degree polynomial regression between the scores of 0, or the number of submerged CRTs due to marine erosion, and the bedrock slope (Fig. 8A). This curvilinear relationship means an increase in the efficiency of erosion up to a threshold at α = 30%, where the number of CRTs completely eroded no longer increases significantly with the slope (Fig. 8A). The same threshold is observed with the relationship between the minimum erosion rate for a completely emerged CRT and the bedrock slope, i.e., the rate decreases as the slope increases until it becomes stable around α = 30% (Fig. 8B).

447

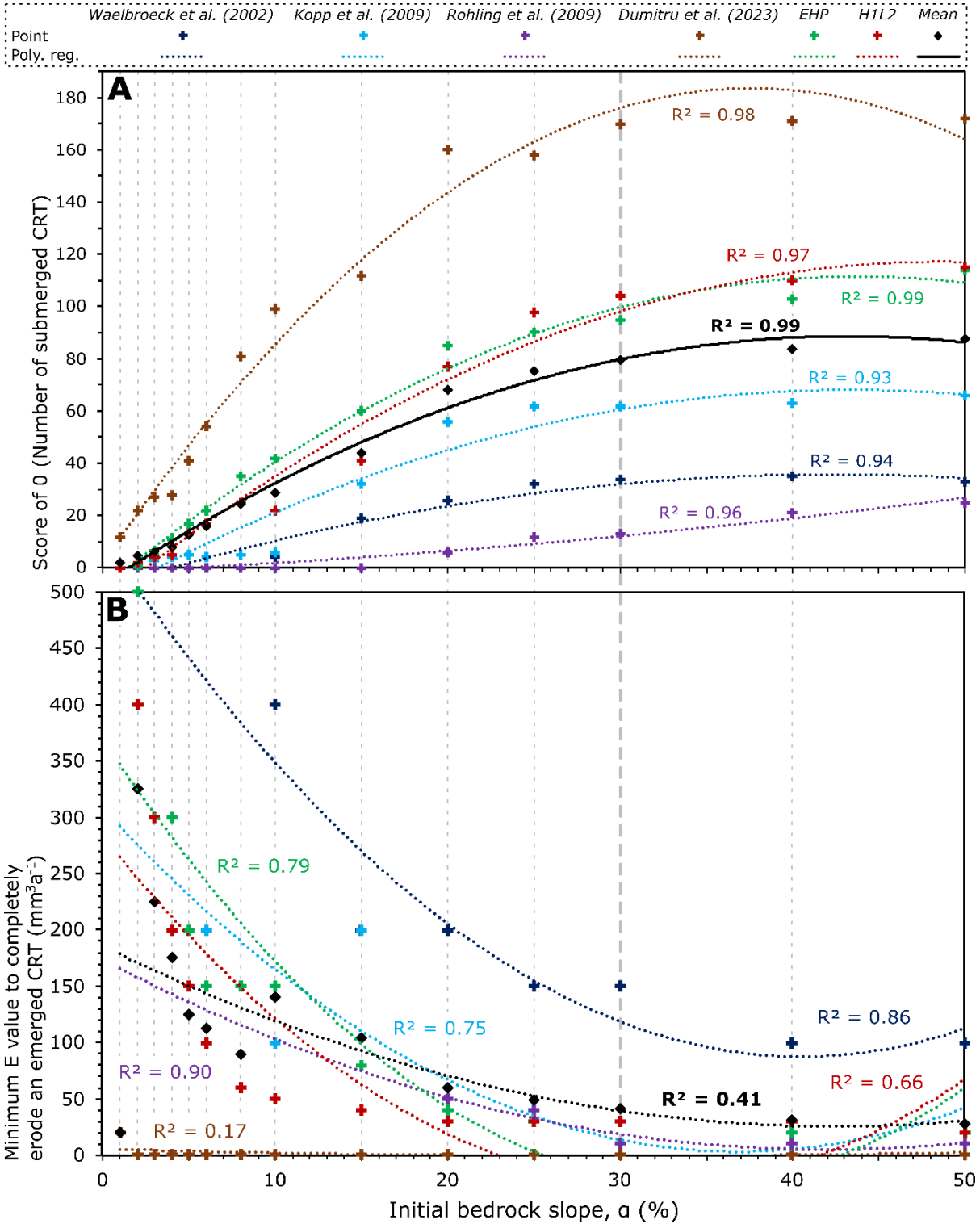
Waelbroeck et al. (2002)
Kopp et al. (2009)
Rohling et al. (2009)
Dumitru et al. (2023)
EHP
H1L2
Mean
Point
Poly. reg.
A
B
Score of 0 (Number of submerged CRT)
Minimum E value to completely erode an emerged CRT (mm³a⁻¹)
Initial bedrock slope, α (%)
R² = 0.98
R² = 0.97
R² = 0.99
R² = 0.99
R² = 0.93
R² = 0.94
R² = 0.96
R² = 0.79
R² = 0.75
R² = 0.90
R² = 0.17
R² = 0.86
R² = 0.66
R² = 0.41

Figure 8. *Relationship between marine erosion and initial bedrock slope (α).* ***A)*** *Polynomial regression between the number of submerged CRT (i.e., fully eroded, score of 0) and the initial bedrock slope (α).* ***B)*** *Polynomial regression between the minimum value of the marine erosion rate (E) to fully erode the CRT and the initial bedrock slope (α). The relationships from the synthetic sea-level scenarios 1P, LHP, LL1A2, 2P, L1H2, L1SLFA2, 3P and 4P are not shown because none of the simulations from them have a score of 0 or, in other words, show any completely eroded CRTs. On the other hand, because no CRTs emerged at more than one meter relative to the present mean sea level, the results from the GMSL curves of Bintanja et al. (2005) and Spratt & Lisiecki (2016) are not considered. "Mean" corresponds to the average value of the sea-level scenarios selected in these relationships (i.e., Waelbroeck et al., 2002; Kopp et al., 2009; Rohling et al., 2009; Dumitru et al., 2023; EHP; H1L2). The bold dotted grey line marks the threshold at α = 30%.*

5. Discussion

In this section, we discuss the limitations of the modelling approach we employed, the realism of the parametric ranges used as input in the model, and the significance of the results in terms of GMSL fluctuations during MIS 5e.

5.1. Limitations

It is important to note the limitations of the REEF model. First and foremost, we assume a linear initial bedrock slope, whereas it is highly unlikely that terraced landscapes begin with a linear topography. Then, the marine erosion rate is based on the wave erosion model of Anderson et al. (1999). It basically represents exponential wave force decay with the landward distance (or decreasing depth), while most recent rock coast studies show much more complicated wave transformations across platforms (e.g., considering the influence of infragravity waves on cliff retreat; Dickson et al., 2013). Also, the model does not take into account subaerial erosion. Moreover, the model cannot simulate the reef facies changes that are observed in most of the cases of multiple reef stratigraphies (e.g., the reef crest demise described by Blanchon et al., 2009 for the Yucatan Peninsula, Mexico). In the same vein, we have set the maximum and optimal depths for reef growth and the maximum depth of wave erosion at 20 m, 2 m, and 3 m respectively (Table 1), although these values can obviously vary locally. Finally, the time step of the model (1 ka) prevents the study of reef formation on short time scales (centennial to annual).

However, it is important to note that despite all the uncertainties of the REEF model, this work is part of an ongoing international effort to develop new constraints, techniques, and approaches (e.g., de Gelder et al., 2022, 2024; Boyden et al., 2023; Rovere et al., 2023). In addition, emerged fossil

coral reefs remain full-fledged geological objects which have already proven their usefulness in understanding past sea-level oscillations for more than a century (e.g., Darwin, 1842; Daly, 1915; Pirazzoli et al, 1991; Rovere et al., 2016; Pedoja et al., 2018; Dumitru et al., 2023).

5.2. Real-world accuracy of parametric ranges

The minimum value of the maximum reef growth rate used in this study (i.e., G_{max} = 1 mm a^{-1}) corresponds to some shallow-water coral reefs in the Caribbean and Indo-Pacific (Dullo, 2005). The maximum value of reef growth rate deduced from specific reef studies is usually between 10- and 15-mm a^{-1} (Macintyre et al., 1977; Adey, 1978, Chappell, 1980; Davies & Hopley, 1983; Bosscher & Schlager, 1992; Dullo, 2005), whereas the one of this study is 50 mm a^{-1}. This high value was used to test extreme cases in which the reef would consist almost exclusively of fast-growing corals (e.g., *Acropora sp.*, Dullo, 2005) which saturate the accommodation space (Camoin & Webster, 2015). However, we consider less realistic the simulations with a maximum reef growth rate higher than 15 mm a^{-1}.

Studies using the REEF model have implemented marine erosion rate (E) values ranging from 20 mm^3 a^{-1} (Pastier et al., 2019), 30 mm^3 a^{-1} (de Gelder et al., 2022), 60 mm^3 a^{-1} (Chauveau et al., 2023) to 360 mm^3 a^{-1} (de Gelder et al., 2023). However, the lack of constraints from marine

erosion affecting coral reefs on millennial scales (Chauveau et al., 2021) has led us to use the wide range: E = [1-500] mm^3 a^{-1}.

Initial bedrock slopes of up to 50% are likely. For example, atoll reefs can grow on reef substrates with slopes close to this value (the Maldivian Archipelago, Rovere et al., 2018; Pag-asa Reefs, West Philippine Sea, Janer et al., 2023) but also fringing reefs (up to 25% at Cape Maisí, Cuba, Authemayou et al., 2023). On the other hand, coral reefs can grow on very gentle slopes (e.g., around 1/2 % for Cockburn Town reef, Bahamas, Chen et al., 1991). Thus, the realism of the chosen parametric set allows us to discuss with confidence the relative importance of each parameter, process, and GMSL scenario on the morphogenesis of the MIS 5e coral reefs.

5.3. MIS 5e multiple-stepped coral reef

Our simulations, which have a score of 2 or more (15% of the 49980 simulations), present two major groups: those in which the reef has not saturated the accommodation space and those in which it has. The first group includes backstepped reefs (whether reoccupied; Figs., 5; 6A; 7B, 7C, 7F) and reefs that follow sea-level changes without ever filling the accommodation space (Figs. 6C; 7A, 7D, 7G, 7H). The second group comprises multiple CRTs that are formed either solely by erosion (Figs. 6B; 7E) or by reefs built on the foreslopes of CRTs that have already emerged (e.g., all the simulation with a value of G_{max} > 8 mm a^{-1} with the 3 peaks

542 synthetic scenario, Fig. SI4). The two groups may differ completely in the
543 processes involved in reef morphogenesis, but their final morphology can
544 be very similar (Fig. 7A, 7D).
545
546 The GMSL curve of Rohling et al. (2009) is the only curve used in this study
547 to successfully simulate a younger CRT on top of an older one through a
548 backstepping process (Figs. 1; 6A). Three other scenarios were close to
549 success but failed (Rohling et al., 2019, LL1A2 and L1SLFA2; Figs. 2; 7B,
550 7C, 7F). As a result, it seems that the only eustatic explanation for creating
551 a proper emerged MIS 5e backstepped reef, in a tectonically stable area, is
552 an abrupt rise in sea level followed by a short-term peak.
553
554 The rate of this rise must be higher (at least 5 mm a^{-1} in our study, LL1A2
555 scenario, Fig. 2B) than the local reef growth rate (no more than 1 mm a^{-1}
556 in our study, Figs. 6A; SI1) to drown the first CRT (Camoin & Webster,
557 2015). The second peak must be short to avoid any reoccupation of the first
558 CRT (no more than 2 ka in our study, Section 4.1., Fig. 7), as must the
559 following regression so as not to completely erode it.
560
561 A drop in sea level between the two peaks (as at 118 ka with the L1SLFA2
562 scenario, Fig. 2C) seems counter-productive to reproduce a backstepped
563 fossil reef because, during it, the previously emerged CRT will be potentially
564 eroded. To our knowledge, the site near Xcaret (Yucatan, Mexico; Blanchon
565 et al., 2009; Blanchon, 2010) is the only one outcropping a MIS 5e

566 backstepped reef in a stable area. As a result, the MIS 5e backstepped reefs
567 simulated with the REEF model (Figs. 5; 6A; 7B, 7C, 7F) appear to have
568 only this real equivalent.
569
570 For the other two scenarios that reach a score of 3, L1H2 and 1P, it is not
571 GMSL fluctuation that entirely explains the formation of a younger CRT on
572 top of an older one, but mostly marine erosion. More specifically, its
573 capacity to dismantle reefal limestone units and cause older ones to emerge
574 (Chauveau et al., 2021; Stout et al., 2023), specifically during sea-level
575 regression (Fig. 6B, 6C, 6D; Chauveau et al., 2023).
576
577 To conclude, a wide range of sea-level scenarios can form multiple
578 stratigraphies with an equally wide range of processes: GMSL fluctuations
579 (Figs., 6A; 7B, 7C, 7F) and marine erosion (Fig., 6B), or the combination of
580 both (Figs., 6C; 7A, 7D, 7E, 7G, 7H). This approach aligns with the recent
581 contributions of Georgiou et al. (2024) who extracted diverse sea-level
582 scenarios through the simulation of erosional RSL indicators (i.e. tidal notch
583 geometry) by combining various parameters affecting their development.
584 Although we cannot conclude whether there were abrupt changes in GMSL
585 during the MIS 5e, we can state that **1)** the GMSL at MIS 5e must have
586 been higher than 2 m (= the optimal reef growth depth, Table 1) to build
587 reefs that are now emerged in tectonically stable areas and **2)** that marine
588 erosion should be systematically considered when establishing the chrono-
589 stratigraphy of fossil coral reefs and the resulting RSL reconstructions.

6. Conclusion

It is crucial to constrain the rate of the very likely future sea-level rise. One of the keys to this is to study past interglacial periods, the last of which is: the Marine Isotope Stage 5e. The global mean sea level at that time may well have fluctuated rapidly, as numerous multiple-stepped stratigraphies around the world seem to testify. These come particularly from fossil coral reefs in tectonically stable areas.

Here, by meticulously analyzing nearly 50 thousand simulations from a coral reef evolution numerical model, we assess the realistic parametric conditions and sea-level scenarios under which such stratigraphies can be generated. Although this model has some limitations, our results show that the only eustatic explanation for emerged backstepped fossil coral reefs (as in the Yucatan Peninsula, Mexico) is a first sea-level peak followed by a period of stabilization or decline, an abrupt rise in sea level and a second short-term peak. There is no need, however, to invoke such abrupt sea-level fluctuations to form other types of multiple-stepped coral reef stratigraphy. Indeed, we emphasize the interactions between bedrock slope, reef growth, and marine erosion. The latter can be a major shaping agent, as it can strip recent reefal limestone units to expose older ones, leading to chrono-morpho-stratigraphies that can be misinterpreted.

Finally, all the conclusions drawn in this study could be improved by further analyses using stratigraphic forward models for specific sites.

Acknowledgements

This project has received funding from the European Research Council (ERC) under the European Union's Horizon 2020 research and innovation programme (grant agreement No.802414). We would like to thank Dr. Anne-Morwenn Pastier for her explanations and help with the REEF model and for the fruitful discussions. With regard to the image shown in Figure 1A, we would like to thank the following projects (conducted by Dr. Christine Authemayou) which enabled Dr. Denovan Chauveau to carry out fieldwork in south-east Cuba and take this photography: "This fieldwork was supported by public funds received in the framework of GEOSUD (DINAMIS), a project (ANR-10-EQPX-20) of the program "*Investissements d'Avenir*" managed by the French National Research Agency. It was also supported by the ISblue project, Interdisciplinary graduate school for the blue planet (ANR-17-EURE-0015) and co-funded by a grant from the French government under the program "*Investissements d'Avenir*" embedded in France 2030 (VuCoRem project, C. Authemayou) and the CNES TOSCA program (CETTROPICO, C. Authemayou)."

Supplementary Information

All 49980 simulations analyzed in this study as well as the scoring spreadsheets for each sea-level scenario are available in a ZENODO repository (https://doi.org/10.5281/zenodo.10695610). A description of the published GMSL curves used in this study can be found in Section SI.1. A description of all the simulations output by the model can be found in Section SI.2. We separated those obtained from proxy-based GMSL scenarios (Section SI.2.1.) from those obtained with the synthetic sea-level curves (Section SI.2.2.). We also present four figures (Figs. SI1; SI2; SI3; SI4) showing the overall scores for each of the 44100 simulations analyzed here.

References

1. Adey W (1978) Coral reef morphogenesis: a multi-dimensional model. Science 202:831–837.
2. Anderson, R.S., Densmore, A.L. & Ellis, M.A. (1999) The generation and degradation of marine terraces. Basin Research, 11(1), 7–20. Available from: https://doi.org/10.1046/j.1365-2117.1999.00085.x
3. Barlow, N. L., McClymont, E. L., Whitehouse, P. L., Stokes, C. R., Jamieson, S. S., Woodroffe, S. A., ... & Sanchez-Montes, M. L. (2018). Lack of evidence for a substantial sea-level fluctuation within the Last Interglacial. Nature Geoscience, 11(9), 627-634.
4. Barnett, R. L., Austermann, J., Dyer, B., Telfer, M. W., Barlow, N. L., Boulton, S. J., ... & Creel, R. C. (2023). Constraining the contribution of the Antarctic Ice Sheet to Last Interglacial sea level. Science Advances, 9(27), eadf0198.
5. Blanchon, P. (2010). Reef demise and back-stepping during the last interglacial, northeast Yucatan. Coral Reefs, 29(2), 481-498.
6. Blanchon, P., Eisenhauer, A., Fietzke, J., & Liebetrau, V. (2009). Rapid sea-level rise and reef back-stepping at the close of the last interglacial highstand. Nature, 458(7240), 881-884.
7. Bintanja, R., Van De Wal, R. S., & Oerlemans, J. (2005). Modelled atmospheric temperatures and global sea levels over the past million years. Nature, 437(7055), 125-128.

671 **8.** Bosscher, H. & Schlager, W. (1992) Computer simulation of reef growth.
672 Sedimentology, 39(3), 503–512. Available from: https://doi.org/10.
673 1111/j.1365-3091.1992.tb02130.x
674 **9.** Boyden, P., Weil-Accardo, J., Deschamps, P., Godeau, N., Jaosedy, N.,
675 Guihou, A., ... & Rovere, A. (2022). Revisiting battistini: Pleistocene coastal
676 evolution of southwestern madagascar. Open Quaternary, 8(1), 1-17.
677 **10.** Bruggemann, J. H., Buffler, R. T., Guillaume, M. M., Walter, R. C., von Cosel,
678 R., Ghebretensae, B. N., & Berhe, S. M. (2004). Stratigraphy,
679 palaeoenvironments and model for the deposition of the Abdur Reef
680 Limestone: context for an important archaeological site from the last
681 interglacial on the Red Sea coast of Eritrea. Palaeogeography,
682 Palaeoclimatology, Palaeoecology, 203(3-4), 179-206.
683 **11.** Camoin, G. F., & Webster, J. M. (2015). Coral reef response to Quaternary
684 sea-level and environmental changes: State of the science. Sedimentology,
685 62(2), 401-428.
686 **12.** Chappell, J. Geology of Coral Terraces, Huon Peninsula, New Guinea: A
687 Study of Quaternary Tectonic Movements and Sea- sevel Changes. GSA
688 Bulletin 85, 553–570 (1974).
689 **13.** Chappell, J. (1980). Coral morphology, diversity and reef growth. Nature,
690 286(5770), 249-252.
691 **14.** Chauveau, D., Authemayou, C., Pedoja, K., Molliex, S., Husson, L., Scholz,
692 D., ... & Aster Team. (2021). On the generation and degradation of emerged
693 coral reef terrace sequences: First cosmogenic 36Cl analysis at Cape Laundi,
694 Sumba Island (Indonesia). Quaternary Science Reviews, 269, 107144.
695 **15.** Chauveau, D., Pastier, A. M., de Gelder, G., Husson, L., Authemayou, C.,
696 Pedoja, K., & Cahyarini, S. Y. (2023). Unravelling the morphogenesis of
697 coastal terraces at Cape Laundi (Sumba Island, Indonesia): insights from
698 numerical models. Earth Surface Processes and Landforms.
699 **16.** Chen, J. H., Curran, H. A., White, B., & Wasserburg, G. J. (1991). Precise
700 chronology of the last interglacial period: 234U-230Th data from fossil coral
701 reefs in the Bahamas. Geological Society of America Bulletin, 103(1), 82-
702 97.
703 **17.** Chutcharavan, P. M., & Dutton, A. (2021). A global compilation of U-series-
704 dated fossil coral sea-level indicators for the Last Interglacial period (Marine
705 Isotope Stage 5e). Earth System Science Data, 13(7), 3155-3178.
706 **18.** Davies, P., Hopley, D. (1983) Growth facies and growth rates of Holocene
707 reefs in the Great Barrier Reef. BMR J Austr Geol Geophys 8:237–251
708 **19.** DeConto, R. M., Pollard, D., Alley, R. B., Velicogna, I., Gasson, E., Gomez,
709 N., ... & Dutton, A. (2021). The Paris Climate Agreement and future sea-
710 level rise from Antarctica. Nature, 593(7857), 83-89.
711 **20.** Deiana, G., Antonioli, F., Moretti, L., Orrù, P. E., Randazzo, G., & Lo Presti,
712 V. (2021). MIS 5.5 highstand and future sea level flooding at 2100 and 2300
713 in tectonically stable areas of central Mediterranean Sea: Sardinia and the
714 Pontina Plain (Southern Latium), Italy. Water, 13(18), 2597.

21. de Gelder, G., Jara-Munoz, J., Melnick, D., Fernández-Blanco, D., Rouby, H., Pedoja, K., ... & Lacassin, R. (2020). How do sea-level curves influence modeled marine terrace sequences?. Quaternary Science Reviews, 229, 106132.

22. de Gelder, G., Husson, L., Pastier, A. M., Fernández-Blanco, D., Pico, T., Chauveau, D., ... & Pedoja, K. (2022). High interstadial sea levels over the past 420ka from the Huon Peninsula, Papua New Guinea. Communications Earth & Environment, 3(1), 256.

23. de Gelder, G., Solihuddin, T., Utami, D. A., Hendrizan, M., Rachmayani, R., Chauveau, D., ... & Cahyarini, S. Y. (2023). Geodynamic control on Pleistocene coral reef development: Insights from northwest Sumba Island (Indonesia). Earth Surface Processes and Landforms, 48(13), 2536-2553.

24. de Gelder, G., Hedjazian, N., Husson, L., Bodin, T., Pastier, A. M., Boucharat, Y., ... & Cahyarini, S. Y. (2024). Reconstructing Quaternary sea-level through bayesian inversion of staircase coastal landscapes. https://doi.org/10.31223/X5B117

25. Dullo, W. C. (2005). Coral growth and reef growth: a brief review. Facies, 51(1-4), 33-48.

26. Dumitru, O. A., Dyer, B., Austermann, J., Sandstrom, M. R., Goldstein, S. L., D'Andrea, W. J., ... & Raymo, M. E. (2023). Last interglacial global mean sea level from high-precision U-series ages of Bahamian fossil coral reefs. Quaternary Science Reviews, 318, 108287.

27. Dutton, A., & Lambeck, K. (2012). Ice volume and sea level during the last interglacial. science, 337(6091), 216-219.

28. Dutton, A., & Barlow, N. L. (2019) What do we know about last interglacial sea level?.

29. Dutton, A., Villa, A., & Chutcharavan, P. M. (2022). Compilation of Last Interglacial (Marine Isotope Stage 5e) sea-level indicators in the Bahamas, Turks and Caicos, and the east coast of Florida, USA. Earth System Science Data, 14(5), 2385-2399.

30. Dyer, B., Austermann, J., D'Andrea, W. J., Creel, R. C., Sandstrom, M. R., Cashman, M., ... & Raymo, M. E. (2021). Sea-level trends across The Bahamas constrain peak last interglacial ice melt. Proceedings of the National Academy of Sciences, 118(33), e2026839118.

31. B. Fox-Kemper, H.T. Hewitt, C. Xiao, G. Aðalgeirsdóttir, S.S. Drijfhout, T. L. Edwards, N.R. Golledge, M. Hemer, R.E. Kopp, G. Krinner, A. Mix, D. Notz, S. Nowicki, I.S. Nurhati, L. Ruiz, J.-B. Sallée, A.B.A. Slangen, Y. Yu, Ocean, cryosphere and sea level change, in Climate Change 2021: The Physical Science Basis. Contribution of Working Group I to the Sixth Assessment Report of the Intergovernmental Panel on Climate Change, V. Masson-Delmotte, P. Zhai, A. Pirani, S.L. Connors, C. Péan, S. Berger, N. Caud, Y. Chen, L. Goldfarb, M.I. omis, M. Huang, K. Leitzell, E. Lonnoy, J.B.R. Matthews, T.K. Maycock, T. Waterfield, O. Yelekçi, R. Yu, B. Zhou, Eds.(Cambridge Univ. Press, 2021), pp. 1211–1362.

759 **32.** Georgiou, N., Geraga, M., Francis-Allouche, M., Christodoulou, D., Stocchi,
760 P., Fakiris, E., et al. (2022). Late Pleistocene submarine terraces in the
761 Eastern Mediterranean, central Lebanon, Byblos: Revealing their formation
762 time frame through modeling. Quaternary International, 638–639, 180–
763 196.
764 **33.** Georgiou, N., Stocchi, P., Casella, E., & Rovere, A. (2023). Decoding the
765 interplay between tidal notch geometry and sea-level variability during the
766 Last Interglacial (Marine Isotopic Stage 5e) high stand. Authorea Preprints.
767 **34.** Hearty, P. J., Hollin, J. T., Neumann, A. C., O'Leary, M. J., & McCulloch, M.
768 (2007). Global sea-level fluctuations during the Last Interglaciation (MIS
769 5e). Quaternary Science Reviews, 26(17-18), 2090-2112.
770 **35.** Hibbert, F. D., Rohling, E. J., Dutton, A., Williams, F. H., Chutcharavan, P.
771 M., Zhao, C., & Tamisiea, M. E. (2016). Coral indicators of past sea-level
772 change: A global repository of U-series dated benchmarks. Quaternary
773 Science Reviews, 145, 1-56.
774 **36.** Horton, B. P., Khan, N. S., Cahill, N., Lee, J. S., Shaw, T. A., Garner, A. J.,
775 ... & Rahmstorf, S. (2020). Estimating global mean sea-level rise and its
776 uncertainties by 2100 and 2300 from an expert survey. NPJ climate and
777 atmospheric science, 3(1), 18.
778 **37.** Husson, L., Pastier, A. M., Pedoja, K., Elliot, M., Paillard, D., Authemayou,
779 C., ... & Cahyarini, S. Y. (2018). Reef carbonate productivity during
780 quaternary sea level oscillations. Geochemistry, Geophysics, Geosystems,
781 19(4), 1148-1164.
782 **38.** Janer, D. F. S., Gabuyo, M. R. P., Carrillo, A. D. V., Co, P. E. Y., del Rosario,
783 A. L. B., Morata, M. J. S., ... & Siringan, F. P. (2023). Development of Pag-
784 asa Reefs, West Philippine Sea: Role of Relative Sea Level Change and Wave
785 Exposure. Philippine Journal of Science, 152(1).
786 **39.** Kennedy, E. V., Roelfsema, C. M., Lyons, M. B., Kovacs, E. M., Borrego-
787 Acevedo, R., Roe, M., ... & Tudman, P. (2021). Reef Cover, a coral reef
788 classification for global habitat mapping from remote sensing. *Scientific*
789 *Data*, *8*(1), 196.
790 **40.** Koelling, M., Webster, J.M., Camoin, G., Iryu, Y., Bard, E. & Seard, C. (2009)
791 SEALEX-internal reef chronology and virtual drill logs from a spreadsheet-
792 based reef growth model. Global and Planetary Change, 66(1–2), 149–159.
793 Available from: https://doi.org/10.1016/j. gloplacha.2008.07.011
794 **41.** Kopp, R. E., Simons, F. J., Mitrovica, J. X., Maloof, A. C., & Oppenheimer,
795 M. (2009). Probabilistic assessment of sea level during the last interglacial
796 stage. Nature, 462(7275), 863-867.
797 **42.** Liu, J., Milne, G. A., Kopp, R. E., Clark, P. U., & Shennan, I. (2016). Sea-
798 level constraints on the amplitude and source distribution of Meltwater Pulse
799 1A. Nature Geoscience, 9(2), 130-134.
800 **43.** Macintyre IG, Burke RB, Stuckenrath R (1977) Thickest recorded Holocene
801 reef section, Isla Perez core, Alacran Reef, Mexico. Geology 5:749–754

44. Matsumoto, H., Young, A. P., & Carilli, J. E. (2022). Modeling the relative influence of environmental controls on marine terrace widths. Geomorphology, 396, 107986.

45. Murray-Wallace, C. V., & Woodroffe, C. D. (2014). Quaternary sea-level changes: a global perspective. Cambridge University Press.

46. O'Leary, M. J., Hearty, P. J., Thompson, W. G., Raymo, M. E., Mitrovica, J. X., & Webster, J. M. (2013). Ice sheet collapse following a prolonged period of stable sea level during the last interglacial. Nature Geoscience, 6(9), 796-800.

47. Pastier, A. M., Husson, L., Pedoja, K., Bézos, A., Authemayou, C., Arias-Ruiz, C., & Cahyarini, S. Y. (2019). Genesis and architecture of sequences of Quaternary coral reef terraces: Insights from numerical models. Geochemistry, Geophysics, Geosystems, 20(8), 4248-4272.

48. Pedoja, K., Husson, L., Johnson, M. E., Melnick, D., Witt, C., Pochat, S., ... & Garestier, F. (2014). Coastal staircase sequences reflecting sea-level oscillations and tectonic uplift during the Quaternary and Neogene. Earth-Science Reviews, 132, 13-38.

49. Pedoja, K., Husson, L., Bézos, A., Pastier, A. M., Imran, A. M., Arias-Ruiz, C., ... & Choblet, G. (2018). On the long-lasting sequences of coral reef terraces from SE Sulawesi (Indonesia): Distribution, formation, and global significance. Quaternary Science Reviews, 188, 37-57.

50. Peñalver, L., Pedoja, K., Martin-Izquierdo, D., Authemayou, C., Nuñez, A., Chauveau, D., ... & Husson, L. (2021). The Cuban staircase sequences of coral reef and marine terraces: A forgotten masterpiece of the Caribbean geodynamical puzzle. Marine Geology, 440, 106575.

51. Pirazzoli, P. A., Radtke, U., Hantoro, W. S., Jouannic, C., Hoang, C. T., Causse, C., & Best, M. B. (1991). Quaternary raised coral-reef terraces on Sumba Island, Indonesia. Science, 252(5014), 1834-1836.

52. Polyak, V. J., Onac, B. P., Fornós, J. J., Hay, C., Asmerom, Y., Dorale, J. A., ... & Ginés, A. (2018). A highly resolved record of relative sea level in the western Mediterranean Sea during the last interglacial period. Nature geoscience, 11(11), 860-864.

53. Raftery, A. E., Zimmer, A., Frierson, D. M., Startz, R., & Liu, P. (2017). Less than 2 C warming by 2100 unlikely. Nature climate change, 7(9), 637-641.

54. Rohling, E. J., Grant, K., Bolshaw, M., Roberts, A. P., Siddall, M., Hemleben, C., & Kucera, M. (2009). Antarctic temperature and global sea level closely coupled over the past five glacial cycles. Nature Geoscience, 2(7), 500-504.

55. Rohling, E. J., Hibbert, F. D., Grant, K. M., Galaasen, E. V., Irvalı, N., Kleiven, H. F., ... & Yu, J. (2019). Asynchronous Antarctic and Greenland ice-volume contributions to the last interglacial sea-level highstand. Nature Communications, 10(1), 5040.

56. Rovere, A., Raymo, M. E., Vacchi, M., Lorscheid, T., Stocchi, P., Gomez-Pujol, L., ... & Hearty, P. J. (2016). The analysis of Last Interglacial (MIS 5e) relative sea-level indicators: Reconstructing sea-level in a warmer world. Earth-Science Reviews, 159, 404-427.

57. Rovere, A., Khanna, P., Bianchi, C. N., Droxler, A. W., Morri, C., & Naar, D. F. (2018). Submerged reef terraces in the Maldivian Archipelago (Indian Ocean). Geomorphology, 317, 218-232.

58. Rovere, A., Ryan, D. D., Vacchi, M., Dutton, A., Simms, A. R., & Murray-Wallace, C. V. (2023). The World Atlas of Last Interglacial Shorelines (version 1.0). Earth System Science Data, 15(1), 1-23.

59. Skrivanek, A., Li, J., & Dutton, A. (2018). Relative sea-level change during the Last Interglacial as recorded in Bahamian fossil reefs. Quaternary Science Reviews, 200, 160-177.

60. Spratt, R. M., & Lisiecki, L. E. (2016). A Late Pleistocene sea level stack. Climate of the Past, 12(4), 1079-1092

61. Thompson, W. G., & Goldstein, S. L. (2005). Open-system coral ages reveal persistent suborbital sea-level cycles. Science, 308(5720), 401-404.

62. Thompson, W. G., Allen Curran, H., Wilson, M. A., & White, B. (2011). Sea-level oscillations during the last interglacial highstand recorded by Bahamas corals. Nature Geoscience, 4(10), 684-687.

63. Toomey, M., Ashton, A.D. & Perron, J.T. (2013) Profiles of ocean island coral reefs controlled by sea-level history and carbonate accumulation rates. Geology, 41(7), 731–734. Available from: https://doi.org/ 10.1130/G34109.1

64. Turcotte, D.L. & Bernthal, M.J. (1984) Synthetic coral-reef terraces and variations of Quaternary sea level. Earth and Planetary Science Letters, 70(1), 121–128. Available from: https://doi.org/10.1016/0012-821X(84)90215-2

65. Veron, J., Stafford-Smith, M., DeVantier, L., & Turak, E. (2015). Overview of distribution patterns of zooxanthellate Scleractinia. Frontiers in Marine Science, 1, 81.

66. Vyverberg, K., Dechnik, B., Dutton, A., Webster, J. M., Zwartz, D., & Portell, R. W. (2018). Episodic reef growth in the granitic Seychelles during the Last Interglacial: implications for polar ice sheet dynamics. Marine Geology, 399, 170-187.

67. Waelbroeck, C., Labeyrie, L., Michel, E., Duplessy, J. C., Mcmanus, J. F., Lambeck, K., ... & Labracherie, M. (2002). Sea-level and deep water temperature changes derived from benthic foraminifera isotopic records. Quaternary science reviews, 21(1-3), 295-305.

68. Webster, J.M., Wallace, L.M., Clague, D.A. & Braga, J.C. (2007) Numerical modeling of the growth and drowning of Hawaiian coral reefs during the last two glacial cycles (0-250 kyr). Geochemistry, Geophysics, Geosystems, 8(3), n/a. Available from: https://doi.org/10.1029/2006GC001415

69. Whitney, B. B., & Hengesh, J. V. (2015). Geomorphological evidence for late Quaternary tectonic deformation of the Cape Region, coastal west central Australia. Geomorphology, 241, 160-174.

Supplementary Information

SI.1. Description of the proxy-based global mean sea level curves

The reconstruction of Waelbroeck et al. (2002) is based on oxygen isotopic ratios of benthic foraminifera from the North Atlantic and Equatorial Pacific Ocean over the last 430 ka and calibrated with the elevation of coral samples corrected from vertical deformation. Thus, Waelbroeck et al. (2002) provide the result of a compilation of several proxies from different parts of the global ocean. Bintanja et al. (2005) used numerical modelling to reconstruct GMSL variations and continental ice volume over 1 Ma from a continuous global compilation of benthic oxygen isotope data. With an extensive compilation of local sea-level indicators (42 localities) and a statistical approach, Kopp et al. (2009) estimated the GMSL from 140 to 90 ka ago. Rohling et al. (2009) used the oxygen isotopic ratios of planktonic foraminifera and bulk sediment from the central Red Sea over 520 ka, while inferring those local variations are roughly representative of GMSL. The meta-analysis of Spratt & Lisiecki (2016) is based on a principal component analysis of earlier compilations (Bintanja et al., 2005; Elderfield et al., 2012; Rohling et al., 2009; Rohling et al., 2014; Shakun et al., 2015; Sosdian & Rosenthal, 2009; Waelbroeck et al., 2002), up to 800 ka. To translate the continuous single-core RSL record of central Red Sea KL11

core (also used in Rohling et al. 2009) to GMSL and to quantify the AIS contributions, Rohling et al. (2019) authors applied apply a first order glacio-isostatic correction and subtract the GIS contribution records (from Yau et al., 2016). Dumitru et al. (2023) presented a RSL MIS 5e record based on high-precision U-series ages of 23 corals collected in the Bahamas archipelago (Crooked Island, Long Cay, Long Island, and Eleuthera). After a strict screening criteria selection of the samples, these authors inferred GMSL from these local data by correcting them for GIA and long-term subsidence (considering a range of ice histories and Earth viscosity structures).

SI.2. Description of all the model outputs.

SI.2.1. Proxy-based GMSL scenarios

The simulations derived from the GMSL curve of Waelbroeck et al. (2002) achieve a maximum score of 1 in the 94% of cases. This means that, with this sea-level scenario, the model did not reproduce any double CRT over the range of parameters used. We note that with a slope of 10% or more and relatively high maximum reef growth rate (G_{max}) and marine erosion rate (E) values, no fossil reefs emerge because they are completely eroded (Fig. SI1). None of the simulations from the GMSL curves of Bintanja et al. (2005) and Spratt & Lisiecki (2016) reach a score higher than 0. This happens because the maximum peak of these curves is less than 1 m

relative to present mean sea level, and therefore less than our limit of 1 m for considering a CRT as emerged (Fig. 1B).

The maximum score reached by the simulations using as sea-level input the GMSL from Kopp et al. (2009) is 2 (Fig. SI1). In fact, while 838 out of 2940 simulations (29%) using this sea-level scenario reproduce multiple CRTs, no simulation originates a younger reef unit above an older one (Fig. SI1). Within the simulations with a score of 2, multiple coral reef morphologies are created only when reef erosion rates (E) fall below 100 mm^3 a^{-1}. Reef growth rates (G_{max}) do not seem to influence in a significant way the scoring, however higher scores are generally achieved with higher rates (10-50 mm a^{-1}). From α = 2%, the emerged CRT starts to disappear (i.e., simulations with a score of 0 are starting to output, Fig. SI1). Scores of 0 are first concentrated at G_{max} = 1 mm a^{-1} up to α = 8%, then gradually widens to all G_{max} values at α = 50%.

Over 2940 simulations using the sea-level curve of Rohling et al. (2009), 523 (18%) attain the highest possible scoring (i.e., 3, Fig. SI1). This score is reached over the entire range of bedrock slopes (α), reef growth rates (G_{max}), and when reef erosion (E) is between 20 to 500 mm^3 a^{-1} (Fig. SI1). Simulations with a score of 2 cover the whole range of G_{max} and E, and from α between 5% to 10%. As the slope and erosion rate increase, the model starts to output more simulations with one single emerged CRT (score of 1, Fig. SI1). Simulations with a score of 0 (no emerged CRT) start at α = 20%

and for values of E = [50-100] mm^3 a^{-1} and G_{max} = [1,2] mm a^{-1}. Scores of 0 increase gradually as α increases. In the end, almost half of the simulations (i.e., 43%) have scores of either 2 or 3, which means that they are characterized by multiple coral reef units during the MIS 5e.

Although the Rohling et al. (2019) GMSL curve is very similar to that of Rohling et al. (2009) (Fig. 2A), the first does not reach a score of 3 (Fig. SI1). This is because the first sea-level peak of the GMSL curve of Rohling et al. (2019) curve (from 128 to 124 ka; Fig. 2A) is 2 ka longer than that of GMSL curve of Rohling et al (2009) (from 129 to 127 ka; Fig. 2A), leading to a systematic reoccupation of the older low terrace (aged of 130-129 ka) by a younger reef (aged of 127/126 ka; Fig. 5B). This therefore invalidates criterion 3 (See Section 4.2. of the main manuscript for further explanation). Although scores of 2 represent 38% of the total simulations, no clear trend emerges (Fig. SI1).

For the GMSL curve of Dumitru et al. (2023), the maximum score is 1 (Fig. SI1), which is reached in 56% of simulations. Simulations with scores of 0 start at α = 1% but only at G_{max} = 1 mm a^{-1}. These increase to higher G_{max} values as the slope increases. From α = 20%, there are only a few simulations with a score of 1 (Fig. SI1).

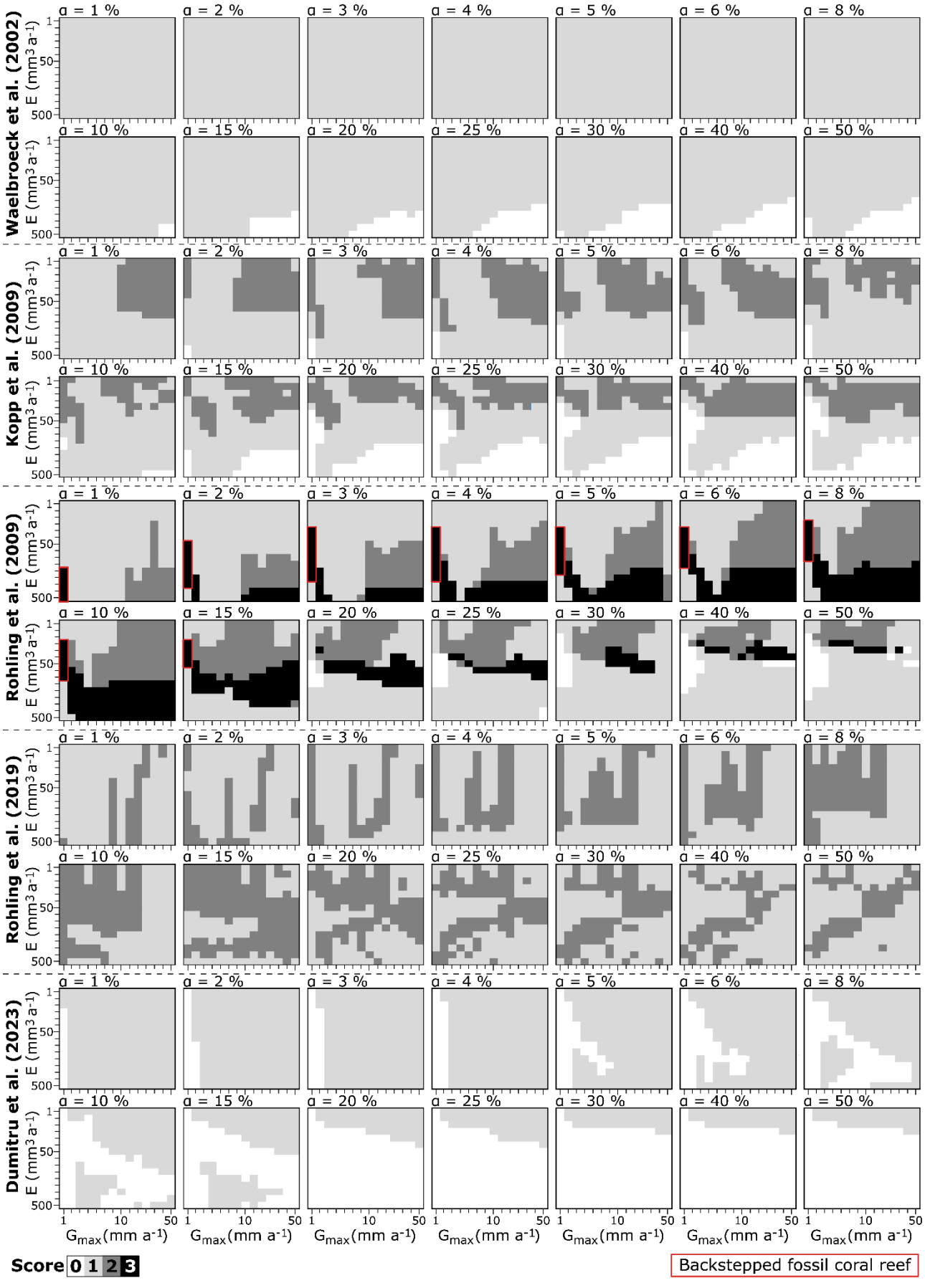
Waelbroeck et al. (2002)
Kopp et al. (2009)
Rohling et al. (2009)
Rohling et al. (2019)
Dumitru et al. (2023)
a = 1 %
a = 2 %
a = 3 %
a = 4 %
a = 5 %
a = 6 %
a = 8 %
a = 10 %
a = 15 %
a = 20 %
a = 25 %
a = 30 %
a = 40 %
a = 50 %
E (mm³ a⁻¹)
1
50
500
1
10
50
Gmax(mm a-1)
Score 0 1 2 3
Backstepped fossil coral reef

979

Figure SI1. *Parametric study of the simulations from published/proxy-based GMSL curves. GMSL curves scenarios (rows), initial bedrock slopes (α, rows and columns), maximum reef growth rates (G_{max}; x axis) and erosion rates (E; y axis). The color of each "small box" represents the score of the simulation for a given parametrization based on the chrono-morphological criteria defined in section 3. Each "medium box" shows simulation scores for the range of G_{max}, and the range of E. Each line of "medium boxes" shows the variability along the range of α. The simulations with a score of 3 correspond to a black square. The results from the GMSL scenarios of Bintanja et al. (2005) and Spratt & Lisiecki (2016) are not shown because none of the simulations derived from them have a score higher than 0.*

SI.2.2. Synthetic SL curves

Here, we describe the results for each synthetic sea-level scenario, i.e., Single- Double- Multi-peak group scenarios (respectively Figs. SI2, SI3, and SI4).

SI.2.2.1. Single-peak scenarios

The maximum score achieved by the one major peak (1P, Fig. 2B) scenario is 3, which is achieved in 6% of the simulations under this sea-level pattern (Fig. SI2). This score is achieved from α = 5% to 50%. From α = 8% to 15%, the scores of 3 cover almost the entire G_{max} range (i.e., G_{max} = [2-50] mm a^{-1} for α = 10%), narrowing to G_{max} = [1-3] mm a^{-1} from α = 25%. Regarding the erosion rate, the maximum scores are constrained to E =

[80-300] mm^3 a^{-1} for α = [5-8]% and then to the range E = [20-300] mm^3 a^{-1} for higher α values (Fig. SI2). Scores of 2 represent only 3% (81 simulations) of the 2940 simulations (Fig. SI2), while scores of 1 represent 91% (2676 simulations).

All the simulations using the Late High Peak (LHP) scenario have a score of 1. This means that, only one emerged CRT is modelled under this scenario.

With an Early High Peak (EHP) the maximum score attained is 1 (Fig. SI2), in 77% of our model runs (2260 simulations). This score represents all simulations at α = 1%. From α = 2%, the model simulates a score of 0 at G_{max} = 1 mm a^{-1} and E = 500 mm^3 a^{-1}. There are more and more 0 scores as α increases. Thus, simulations with a score of 0 represent 54% of all simulations at α = 50%.

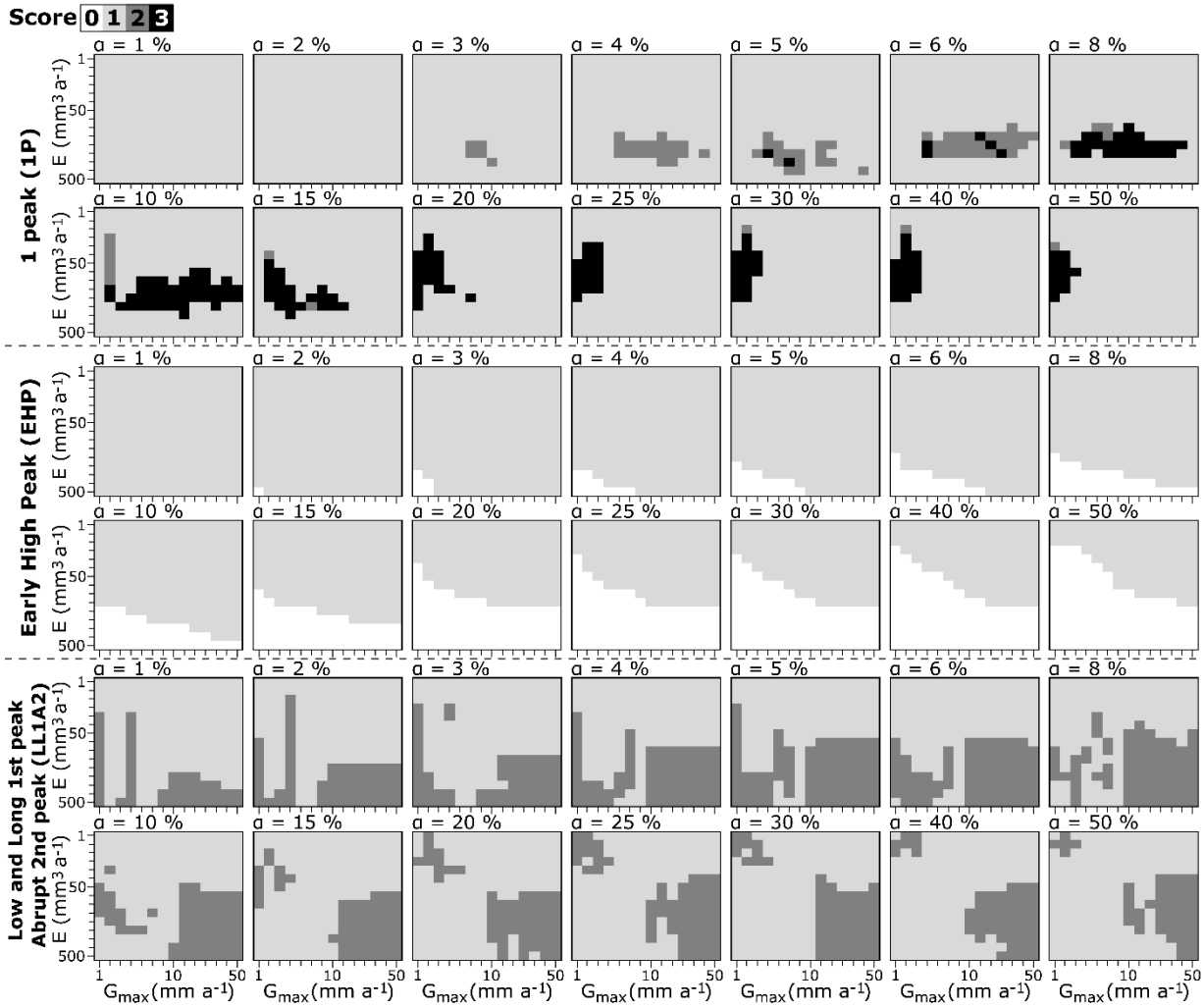

Figure SI2. *Parametric study of the simulations from the synthetic GMSL curves of the single-peak scenario group. Same description as Figure SI1. The results from the Late High Peak (LHP) scenario are not shown because none of the simulations derived from it have a score different than 1.*

Under the sea-level scenario characterized by a Low and Long 1st peak and an abrupt 2nd peak (LL1A2), a score of 2 is attained in 31% of our model runs (921 simulations), while 61% of simulations reach a score of 1 (2019 simulations). The simulations are divided in two groups from α = 1%. The first group is constrained to G_{max} < 6/8 mm a^{-1}, the second concentrated

on values of G_{max} > 6/8 mm a^{-1} and E > 40 mm^3 a^{-1}. These two groups become more distinct as α values increase (Fig. SI2).

SI.2.2.2. Double-peak scenarios

The maximum score of 2 is reached for the two-peaks (2P) sea-level scenario (13% of the total; Fig. SI3). These scores are concentrated around E = 500 mm^3 a^{-1} and low G_{max} values (under 5 mm a^{-1}) at α = 1%. The number of 2-scores increase as the α increases. From α = 15%, there are no longer any simulations with a score of 2 at E = 500 mm^3 a^{-1}. This trend continues at lower erosion rate values until E = 50 mm^3 a^{-1} for α = 50%. Also, from α = 40%, there are no more scores of 2 at G_{max} = 1 mm a^{-1}. The score of 3 has almost been reached by 2P, with a younger reefal limestone unit sometimes emerging above an older one, but the separation between the two is not morphologically significant enough to consider that they form two distinct units.

The maximum score of 3 is reached by the Low 1st peak, High 2nd peak (i.e, L1H2) scenario (1% of total; Fig. SI3). These scores are only concentrated at G_{max} = [1,2] mm a^{-1} and at E > 80 mm^3 a^{-1}. The scores of 2 seem to show the same trend as those of scenario 2P, i.e., concentrated almost over the whole E range and G_{max} = [1-6] mm a^{-1} from α = [1-5] %. There are fewer and fewer scores of 2 as α increases. At α = 50% only 1 simulation with a score of 2 remain.

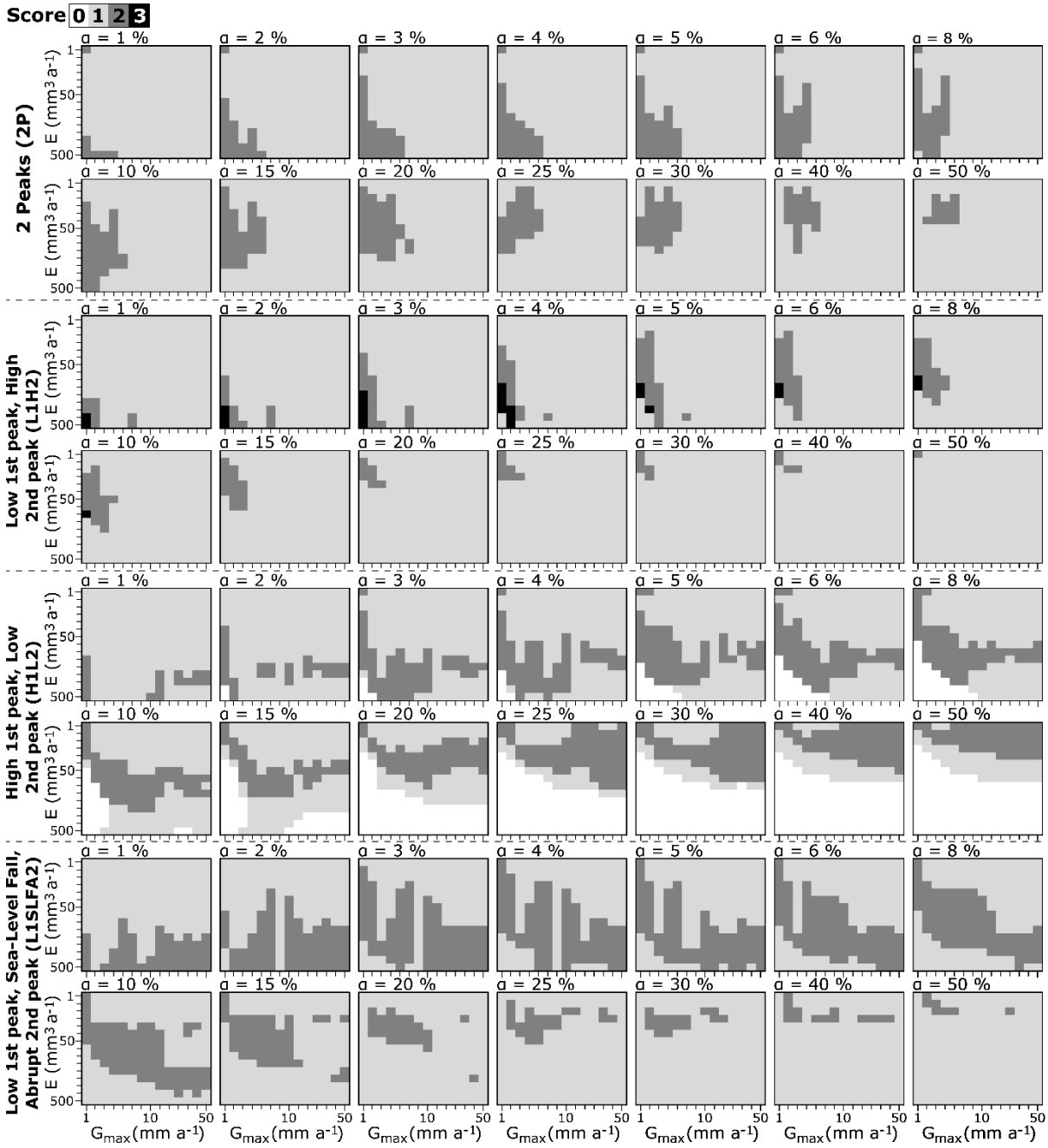

Figure SI3. *Parametric study of the simulations from the synthetic GMSL curves of the double-peak scenario group. Same description as Figure SI1.*

A maximum score of 2 is attained for the High 1st peak, Low 2nd peak (H1L2) scenario (Fig. SI3). The 2-score simulations are dispersed across the ranges of E and G_{max}. These are concentrated around E = [100-500] $mm^3\ a^{-1}$ at α = 1%, whereas they are partitioned around E = [1-30] $mm^3\ a^{-1}$ α = 50%.

At α = 2%, there are two simulations with a score of 0 (Fig. SI3). The number of simulations with a score of 0 increases as the slope increases. At α = 50%, these scores represent 55% of the 210 simulations (Fig. SI3).

The last sea-level scenario of group II (i.e., Low 1st peak, Sea-Level Fall, Abrupt 2nd peak, L1SLFA2), attained the maximum score of 2 (Fig. SI3). These scores are concentrated for almost all G_{max} value ranges and below E = 80 mm^3 a^{-1} at α = 1%. The number of simulations with a score of 2 decreases as α values increase. Thus, the scores of 1 represent almost the entire range of simulation at α = 50% (~95% of the 210 simulations, Fig. SI3).

SI.2.2.3. Multi-peak scenarios

The maximum score of 3 is not reached by either the 3-peaks (3P) or 4-peaks (4P) scenario, only scores of 1 and 2 (Fig. SI4). For the 3P scenario, there are two distinct groups of 2-scores (525 simulations, 18% of total) for values of α = [1-15] %, one concentrated on values of G_{max} < 8 mm a^{-1} and the other at G_{max} > 8 mm a^{-1}. At α > 15 %, the scores of 2 are concentrated at G_{max} < 5 mm a^{-1} and E < 60 mm^3 a^{-1}. For the 4P scenario, scores of 2 (477 simulations, 16% of total) also seem to form the same two groups as those highlighted by 3P (Fig. SI4).

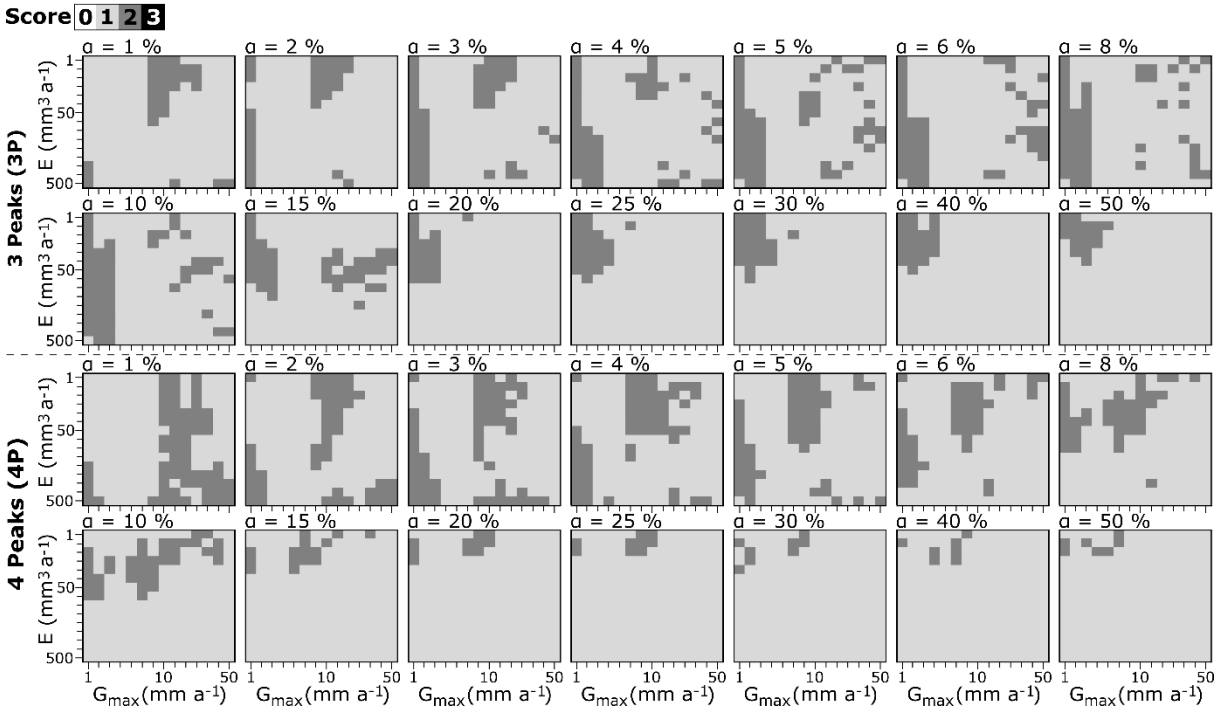

Figure SI4. *Parametric study of the simulations from the synthetic GMSL curves of the multi-peak scenario group. Same description as Figure SI1.*